The acetylene spectrum in the 1.45 μm window (6 627–70 65 cm –1)

Oleg Lyulin, Semyon Vasilchenko, Didier Mondelain, Samir Kassi, Alain Campargue

Manuscript Details

Manuscript number	JQSRT_2020_189
Title	The acetylene spectrum in the 1.45 μm window (6627-7065 cm–1)
Article type	Full Length Article

Abstract

The high-resolution absorption spectrum of acetylene has been recorded at room temperature by high sensitivity cavity ring down spectroscopy (CRDS) in the 6627-7065 cm–1 region. The studied spectral range corresponds to a spectral interval of very weak absorption (an acetylene transparency window). The positions and intensities of more than 7000 lines are determined in the considered interval where previous intensity information was mostly missing. On the basis of previous studies and on effective Hamiltonian predictions, 3062 12C2H2, 462 12C13CH2 and 104 12C2HD absorption lines belonging to a total of 123 vibrational bands are assigned. For comparison, the HITRAN2016 database provides line parameters of only ten 12C2H2 bands in the same region. Spectroscopic parameters of 113 upper vibrational levels were derived from standard band-by-band fits of the line positions (typical rms values of the (obs.-calc.) deviations are better than 0.003 cm–1). Many bands are found to be affected by perturbations. The vibrational transition dipole moment squared and Herman-Wallis coefficients of 47 bands were derived from a fit of the measured intensity values. In order to generate a recommended line list in the region, the derived spectroscopic parameters and Herman-Wallis coefficients were used to compute the line parameters for these 47 bands while experimental position and intensity values were kept for the other bands. Overall, the obtained recommended list including a total of 5260 transitions will help to fill a spectral gap around 1.47 μm where very scarce spectroscopic information is provided in the current spectroscopic databases. When compared to the HITRAN list in the region, some important deviations concerning both line positions and line intensities are evidenced as a result of inaccurate high J extrapolations.

Keywords	acetylene; C2H2; line intensity; CRDS; spectroscopic database; HITRAN

Corresponding Author	alain Campargue
Corresponding Author's Institution	cnrs
Order of Authors	Oleg Lyulin, Semyon Vasilchenko, Samir Kassi, Didier Mondelain, alain Campargue
Suggested reviewers	david jacquemart, Jean Vander Auwera, Severine Robert

Submission Files Included in this PDF

File Name [File Type]

Highlights.doc [Highlights]

Graphical abstract.JPG [Graphical Abstract]

21mars.doc [Manuscript File]

all_figs.pptx [Figure]

conflict of interest.docx [Conflict of Interest]

Submission Files Not Included in this PDF

File Name [File Type]

cover-letter.txt [Cover Letter]

SupMat1_SP19Mars.txt [Supplementary Material]

SupMat2_HW fit.txt [Supplementary Material]

SupMat3_recommended19Mars.txt [Supplementary Material]

To view all the submission files, including those not included in the PDF, click on the manuscript title on your EVISE Homepage, then click 'Download zip file'.

Highlights

High sensitivity CRDS of acetylene in the 1.45μm transparency window (6627-7065 cm^{-1})
More than 3600 transitions assigned to 123 bands of $^{12}C_2H_2$, $^{12}C^{13}CH_2$ and $^{12}C_2HD$
Spectroscopic parameters and Herman-Wallis coefficients are derived
A recommended empirical line list of 5260 transitions is generated in the region
Some important deficiencies are evidenced in the HITRAN2016 and ASD lists

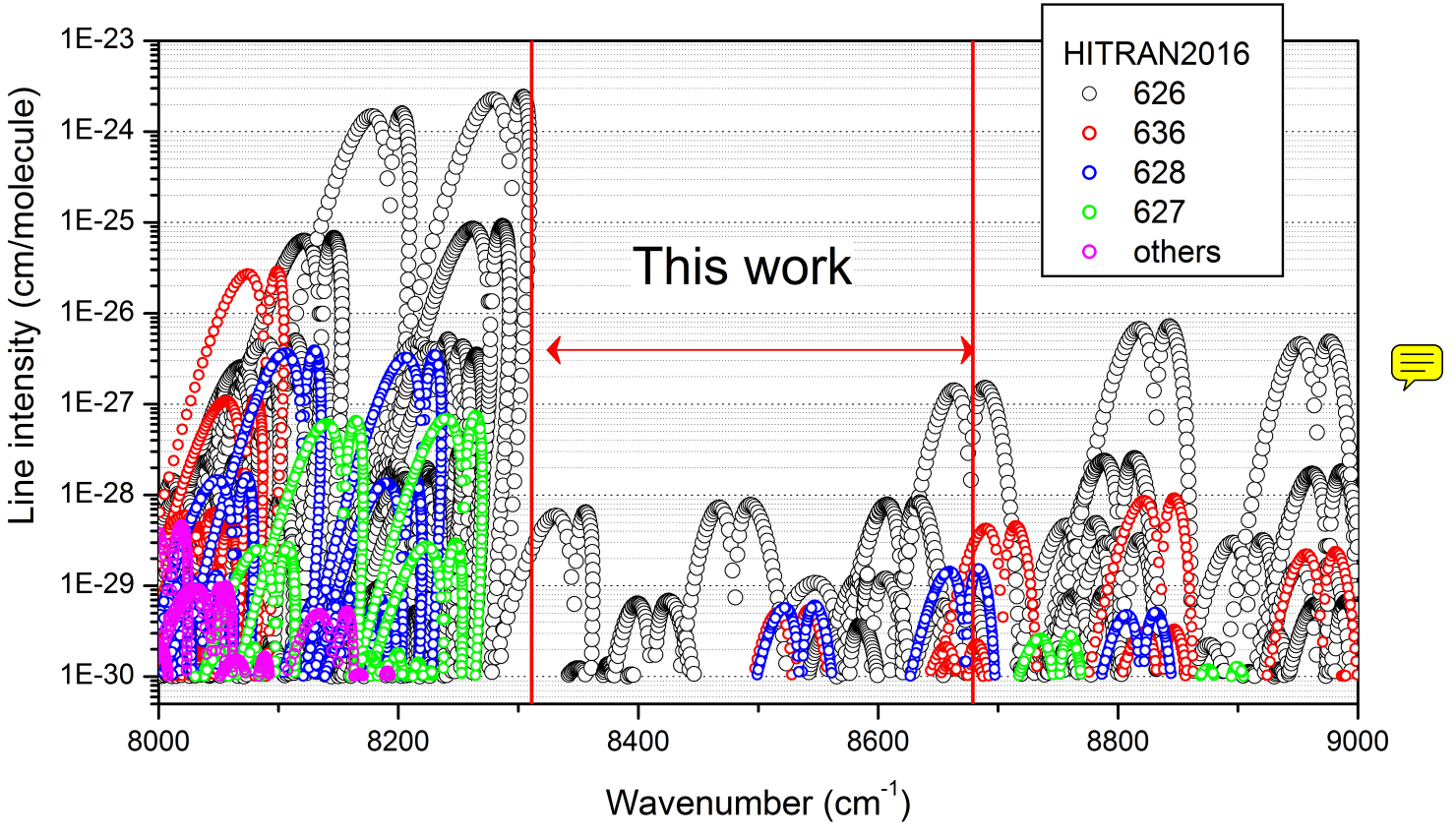
HITRAN2016
626
636
628
627
others
This work
Line intensity (cm/molecule)
1E-23
1E-24
1E-25
1E-26
1E-27
1E-28
1E-29
1E-30
8000
8200
8400
8600
8800
9000
Wavenumber (cm-1)

The acetylene spectrum in the 1.45 µm window (6627-7065 cm^{-1})

O. Lyulin[1,2], S.Vasilchenko[1,2], D. Mondelain[1], S.Kassi [1], Alain Campargue[1*]

[1] Univ. Grenoble Alpes, CNRS, LIPhy, *38000 Grenoble, France*

[2] V.E. Zuev Institute of Atmospheric Optics SB RAS,*1, Academician Zuev square, Tomsk 634055, Russia*

Number of Pages: 29
Number of Figures: 5
Number of Tables: 3

Running Head: *Acetylene near 1.45 µm*

Keywords: *acetylene; C_2H_2; line intensity; CRDS; spectroscopic database; HITRAN*

* Corresponding author
Tel: +33 4 76 51 43 19
E-mail address: Alain.Campargue@univ-grenoble-alpes.fr

Friday, March 20, 2020

ABSTRACT

The high-resolution absorption spectrum of acetylene has been recorded at room temperature by high sensitivity cavity ring down spectroscopy (CRDS) in the 6627-7065 cm^{-1} region. The studied spectral range corresponds to a spectral interval of very weak absorption (an acetylene transparency window). The positions and intensities of more than 7000 lines are determined in the considered interval where previous intensity information was mostly missing. On the basis of previous studies and on effective Hamiltonian predictions, 3062 $^{12}C_2H_2$, 462 $^{12}C^{13}CH_2$ and 104 $^{12}C_2HD$ absorption lines belonging to a total of 123 vibrational bands are assigned. For comparison, the HITRAN2016 database provides line parameters of only ten $^{12}C_2H_2$ bands in the same region. Spectroscopic parameters of 113 upper vibrational levels were derived from standard band-by-band fits of the line positions (typical *rms* values of the (obs.-calc.) deviations are better than 0.003 cm^{-1}). Many bands are found to be affected by perturbations. The vibrational transition dipole moment squared and Herman-Wallis coefficients of 47 bands were derived from a fit of the measured intensity values. In order to generate a recommended line list in the region, the derived spectroscopic parameters and Herman-Wallis coefficients were used to compute the line parameters for these 47 bands while experimental position and intensity values were kept for the other bands. Overall, the obtained recommended list including a total of 5260 transitions will help to fill a spectral gap around 1.47 μm where very scarce spectroscopic information is provided in the current spectroscopic databases. When compared to the HITRAN list in the region, some important deviations concerning both line positions and line intensities are evidenced as a result of inaccurate high *J* extrapolations.

1. Introduction

The present contribution takes part in a long term project aiming at constructing an empirical spectroscopic database for acetylene in the near infrared using Fourier-transform spectroscopy (FTS) in the region of the strong bands and cavity ring down spectroscopy (CRDS) in the weak absorption intervals between the bands (or transparency windows). Indeed, in spite of being the most studied four-atoms molecule and of increasing needs for planetary application[illegible] status of the spectroscopic databases of acetylene (C_2H_2) in the near infrared is far to be satisfactory both in terms of completeness and accuracy. For instance, in its last version, the HITRAN database [1] provides only the few strongest bands for each ΔP variation of the polyad quantum number ($P= 5V_1+3V_2+5V_3+V_4+V_5$, where V_i are the conventional vibrational normal modes quantum numbers, and i= 1-5 correspond to the symmetric CH and CC stretching modes, the antisymmetric CH stretch, and the *trans*- and *cis*-degenerate bending modes, respectively).

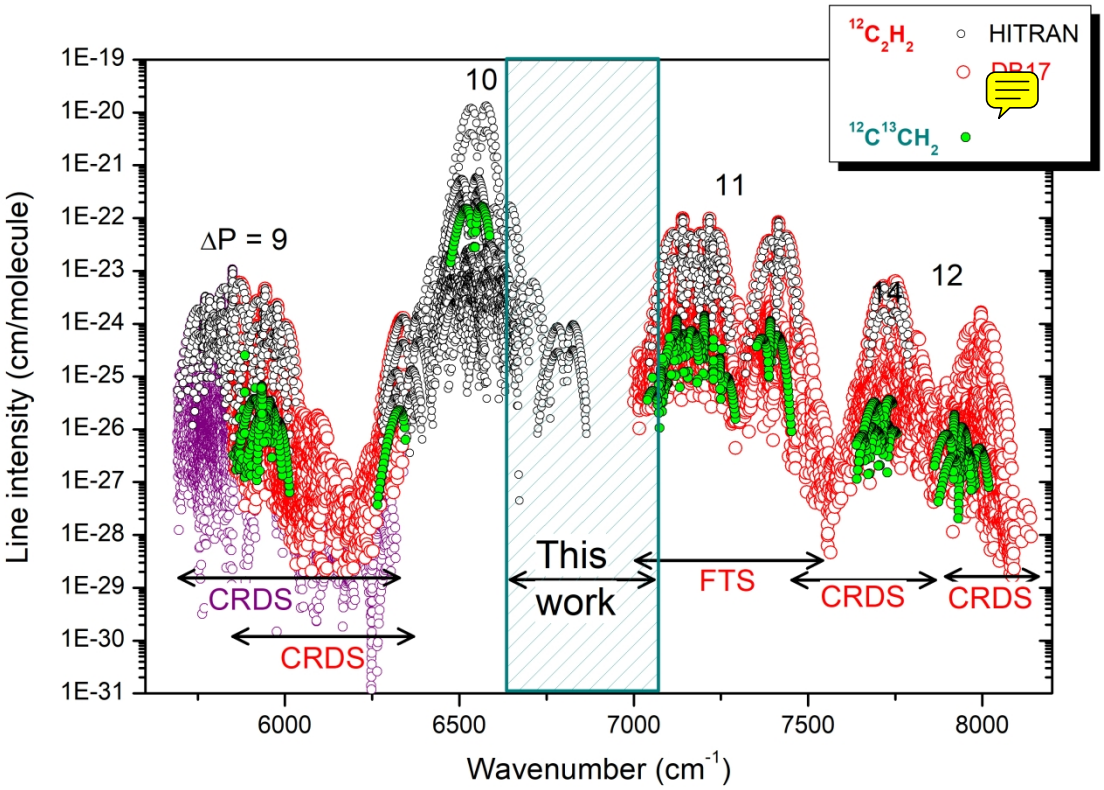

Fig. 1

Overview of the acetylene spectrum between 5600 and 8200 cm^{-1}. The HITRAN2016 line list [1] (black circles) is superimposed to the empirical database of Ref. [2] (red circles). A recent CRDS study has extended the observations in the 5695-6340 cm^{-1} region (violet circles). The $^{12}C^{13}CH_2$ transitions are highlighted (full green circles). The ΔP values of the variation of the polyad quantum number are indicated.

In 2017, we constructed a spectroscopic database (EDB[illegible] hereafter) for acetylene in the wide 5850-9415 cm^{-1} region [2] by gathering results of three FTS studies [3-5] and three CRDS studies [6-8]. Compared to the HITRAN2016 [1] and GEISA2015 [9] spectroscopic databases in the region, the

number of bands and lines was increased by more than a factor of ten. As a rule, in absence of perturbation, the line positions included in the database are empirical values calculated using spectroscopic parameters of the lower and upper energy vibrational levels derived from a band-by-band fit of the measured line positions. Line intensities are computed using the vibrational transition dipole moment squared and Herman-Wallis coefficients derived from band-by-band fits of measured intensity values. In case of perturbation, experimental values are generally preferred. Note that a recent CRDS study in the 5693-5882 cm^{-1} region [10] and a FTS study in the 9280-10740 cm^{-1} interval [11,12] will allow extending the database to lower and higher energies. **Fig. 1** shows an overview of the EDB17 and HITRAN2016 in the 5600-8200 cm^{-1} interval.

As illustrated in **Fig. 1**, the 6341-7000 cm^{-1} interval was excluded from the empirical database of Ref. [2]. This spectral region including the strongest band in the region, namely the $\nu_1+\nu_3$ band centered at 6543 cm^{-1} with line intensities up to 1×10^{-20} cm/molecule, was extensively studied by Keppler et al. [13] by FTS. These authors used a 352.5 m absorption pathlength which allowed them to detect lines with intensity smaller than of 10^{-25} cm/molecule. Keppler's measurements are the main source of line positions for the acetylene HITRAN2016 list in the 6250-6850 cm^{-1} region but no line intensities were provided in Ref. [13]. As detailed in Ref. [14], HITRAN line intensities in the region rely on transition dipole moment and Herman-Wallis coefficients derived from FTS spectra in Refs. [14-17]. Above 6750 cm^{-1}, the HITRAN2016 database does not provide any data up to 7050 cm^{-1} except for the relatively weak $2\nu_1+\nu_5{}^1-\nu_4{}^1$ hot band near 6805 cm^{-1}. Indeed, the 6700-7100 cm^{-1} interval is a region of weak absorption for acetylene which requires ~~a~~ high sensitivity to be characterized. It is formed by weak bands of the high energy range of the $\Delta P = 10$ manifold and on the low energy edge of the $\Delta P = 11$ manifold (see **Fig. 1**). Some years ago, a high number of transitions was assigned in this region from a series of CRDS spectra recorded in our laboratory between 6667 and 7015 cm^{-1} [18,19]. The assignments relied on the global effective Hamiltonian model developed at Université Libre de Bruxelles [20-23]. No intensity information was reported in these CRDS studies.

In the present work, we reconsider these previous CRDS spectra and extend the spectral coverage by new recordings at lower and higher energy (6627-7065 cm^{-1}). Our goal is twofold: *(i)* to provide intensity information requested to incorporate these data in spectroscopic databases and *(ii)* to extend the assignments using the global effective model developed at IAO-Tomsk for $^{12}C_2H_2$ [24,25]. The first step of the analysis is the construction of a global experimental list of about 7000 lines, as described in the following Part 2. The next steps are the rovibrational assignments (a total of 123 vibrational bands were assigned) and the derivation of the spectroscopic parameters of the corresponding upper vibrational levels (Part 3 and 4, respectively). Finally, for 47 bands, the vibrational transition dipole moment squared and Herman-Wallis coefficients could be determined from a fit of the measured intensities (Part 5). Gathering the retrieved position and intensity information, the first recommended empirical line list is proposed for the considered spectral window

of acetylene and compared to the previous data available in the literature for the strongest bands (Part 6).

2. Experimental details and line list construction

The newly recorded spectra cover the 6627-7065 cm^{-1} region including thus the entire 6667-7015 cm^{-1} range analyzed in Refs. [18,19]. Because impurity lines (mostly due to water) were less intense in the previous recordings, the new spectra were mainly used in the low and high energy edges (6627-6702 cm^{-1} and 7015-7065 cm^{-1}, respectively) where the acetylene absorption is stronger.

The reader is referred to Refs. [26,27] for a general description of the CRDS setups used for the recordings. Fibered distributed feed-back (DFB) laser diodes were used as light sources. Each laser diode frequency range is about 30 cm^{-1} by temperature tuning from -5°C to 60°C. Overall a total of fourteen DFB lasers were needed to cover the region A few hundreds ring down events were averaged for each spectral data point, and the duration of a temperature scan was about 100 minutes for each DFB laser.

The cell was filled with acetylene (from Air Liquide) of normal isotopic abundance. The gas pressure was continuously measured by capacitance gauges (MKS Baratron, 1, 10 and 100 Torr, 0.25 % accuracy of the reading). The pressure values used in the recordings of Refs. [18,19] were 5.0, 10.0 and 20.0 Torr. Lower pressure values (0.1 and 1. Torr) were adopted for the new recordings in the low and high energy edges of the window correspond to relatively strong absorption. The cell temperature was measured with a temperature sensor (TSic 501, IST-AG, 0.1 K accuracy) fixed on the cell surface, covered by an external blanket of foam for thermal isolation. During the recordings reported here, the cell temperature varied between 294.3 and 296.1 K.

During the spectra recordings, a wavemeter measured the wavenumber of the laser emission at each spectral step of typically 0.002 cm^{-1} giving a first frequency calibration of the spectrum. This calibration was then refined using accurate line positions of water vapor (desorbing from the walls of the cell), provided in the HITRAN2016 database [1]. This leads to an estimated uncertainty of 1-2×10^{-3} cm^{-1} on the line center determination of unblended lines.

The minimum detectable absorption coefficient (evaluated as the *rms* of the base line fluctuation), α_{min}, varies between 1×10^{-10} cm^{-1} and 6×10^{-11} cm^{-1} depending on the RD time. As a result, line intensities spanning more than three orders of magnitude (from 5×10^{-24} to 2×10^{-28} cm/molecule) could be retrieved from the measured spectra. The successive enlargements of the spectra presented in **Fig. 1** illustrate the sensitivity and high dynamic range of the recordings and the noise level on the order of $\alpha_{min}\sim 7\times10^{-11}$ cm^{-1}. It is worth mentioning that, at this sensitivity level, the main limitation for the spectrum assignment is the very high spectral congestion (about 20 lines/cm^{-1}) and the absence of sufficiently accurate predictions. As a result, the rovibrational assignment procedure was particularly laborious and a large number of detected lines remained unassigned (see below).

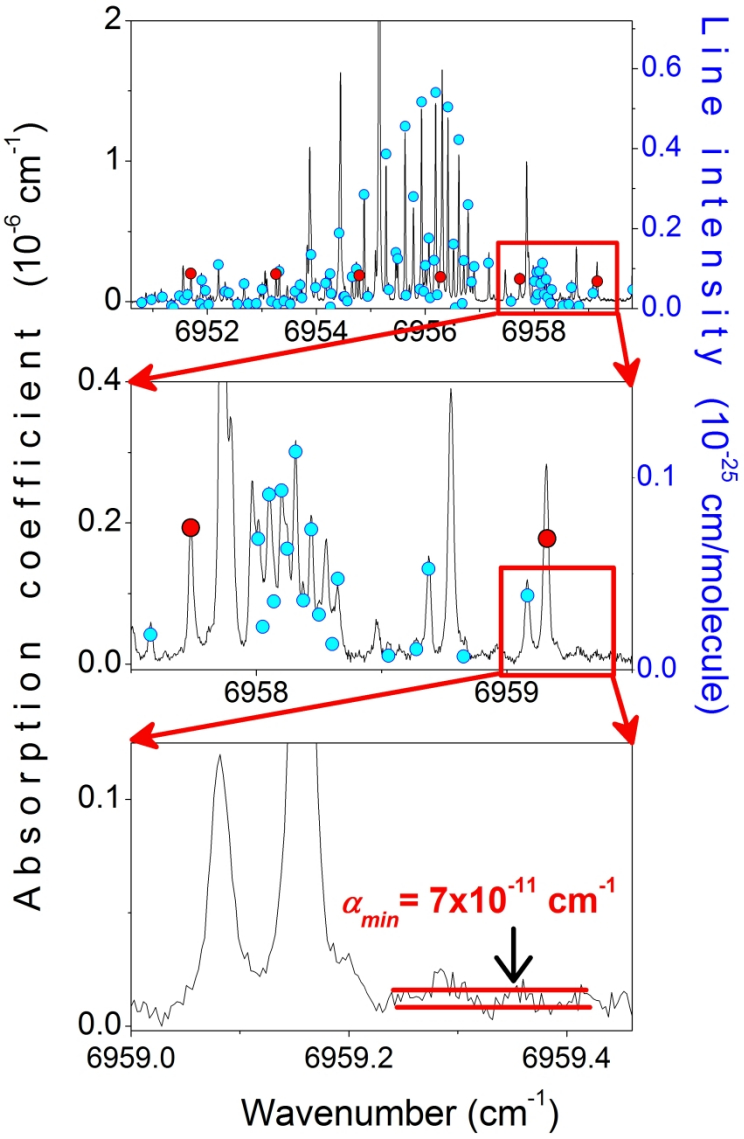

Fig. 2
CRDS spectrum of acetylene near 6959 cm^{-1}. The sample pressure was 20.0 Torr. The enlargements illustrate the high dynamics of the recordings giving access to absorption coefficients from 10^{-6} cm^{-1} to the noise level α_{min}~ 7×10^{-11} cm^{-1}. The blue and red dots correspond to the recommended line list constructed in this work for $^{12}C_2H_2$ and $^{12}C_2HD$, respectively. A number of lines due to water present as an impurity are superimposed to the acetylene spectrum. In the region of the upper panel, the spectrum is dominated by the *Q* branch of the $2\nu_3+2\nu_4^0-\nu_5^1$ $\Sigma_g^+-\Pi_u$ band centered at 6956.923 cm^{-1}. The medium panel shows the *Q* branch of the $2\nu_3+3\nu_4^1-(\nu_4+\nu_5)^0$ $\Pi_g-\Sigma_u$ band centered at 6958.350 cm^{-1}. The lines of $^{12}C_2HD$ (in natural isotopic abundance) belong to the *R*-branch of the $\nu_2+2\nu_3$ $\Sigma-\Sigma$ band centered at 6932.193 cm^{-1}.

The elaboration of the global line list was performed using a homemade multiline fitting computer code using a Voigt profile as line shape. As illustrated on **Fig. 2**, the frequent line overlapping and high density of lines made this step particularly laborious. The self-broadening coefficients were varied when needed or otherwise, fixed to a default value of 0.14 cm^{-1}/atm [3]. The resulting line list counts about 8000 lines. In the most favorable cases (well isolated lines of medium intensity), the accuracy of the line positions is estimated to be about 10^{-3} cm^{-1} while the error bar on

the line intensities is estimated to be 3%. Nevertheless, line overlapping degrades the accuracies for a significant fraction of the measurements. After removing some lines too strong to be accurately measured and lines due to water vapor, carbon dioxide and methane identified using the HITRAN database [1], the list was reduced to about 6500 lines which are believed to belong to acetylene. The weakest lines around the center of the window have an intensity on the order of a few 10^{-28} cm/molecule. For comparison, note that some water lines in the region have an intensity larger than 10^{-20} cm/molecule.

3. Rovibrational assignments

In order to rovibrationally assign the measured lines, we first considered literature data. In addition to the HITRAN database [1], the large sets of $^{12}C_2H_2$ assignments published by Robert et al. [18] and Amyay et al. [19] were gathered (about 2600 transitions in total in the investigated region). Lines due to the $^{12}C^{13}CH_2$ and $^{12}C_2HD$ minor isotopologues with (assumed) natural abundances in our sample, were searched using the set of line positions provided in Ref. [28] and Ref. [29], respectively. It is worth mentioning that, in the considered region, no intensity information is available for these species in the literature. 464 and 104 absorption lines were assigned to $^{12}C^{13}CH_2$ and $^{12}C_2HD$, respectively (see **Figs. 2** and **3**). Note that the natural relative concentration of $^{12}C_2HD$ is only about 3×10^{-4}. Finally, the acetylene spectroscopic databank (ASD) [25] limited to the main isotopologue and calculated with a 10^{-28} cm/molecule intensity cut off was considered to extend the $^{12}C_2H_2$ assignments. The ASD was generated on the basis of a global effective Hamiltonian (EH) model developed in the frame of the effective operator approach [24]. This model considers all the resonance interactions between rovibrational levels up to the ninth order of perturbation theory. Effective rovibrational parameters were adjusted to reproduce about 30000 measured line positions collected from the literature up to 9900 cm^{-1}.

Table 1.

Comparison of the number of bands and transitions reported in this work, included in the HITRAN database and in the previous CRDS studies of Refs. [18,19].

	6627-7065 cm^{-1}		6667-7015 cm^{-1}
	This work	HITRAN	Amyay et al. [19]/Robert et al. [18]
	Number of bands		
$^{12}C_2H_2$	105	10	72/15
$^{12}C^{13}CH_2$	15	0	
$^{12}C_2HD$	3	0	
	Number of transitions		
$^{12}C_2H_2$	3304/3685 [a]	397	1497/1200
$^{12}C^{13}CH_2$	464/554 [a]	0	
$^{12}C_2HD$	104/114 [a]	0	

Note.

[a] The first and second numbers correspond to the number of lines measured in this work and included in the recommended list, respectively (Supplementary Material I and III, respectively). Note that these two numbers include some strong lines from HITRAN2016 and from our empirical database [2].

The ASD provides line intensities calculated using a set of effective dipole moment (EDM) parameters for each ΔP value. The spectral region of interest involves ΔP= 10 and ΔP= 11 bands, roughly below and above about 6900 cm^{-1}, respectively. The ΔP= 10 and 11 EDM parameters used for the ASD were fitted in Ref. [24] from FTS intensity values available for the strongest bands in Refs. [15-17] and in Refs. [3,14], respectively (see **Fig. 1**).

Although inaccurate for a fraction of the bands (see below), the ASD intensities provided valuable information to extend the assignments. The presence of a *Q* branch, the observation of the 1:3 intensity alternation from even to odd values of *J* and lower state combination difference (GSCD) relations were systematically used as additional criteria. As a result, 3062 lines were assigned to 105 $^{12}C_2H_2$ bands, 462 lines to fifteen $^{12}C^{13}CH_2$ bands and 104 lines to three $^{12}C_2HD$ bands. A statistic comparison of the assignments with the HITRAN2016 database and Refs. [18,19] is presented in **Table 1**. Our band list is presented in **Table 2** in increasing order of the upper energy level. In the last column, we indicate for each band the reference of previous reports when available. Previous studies include the above mentioned CRDS studies, the long path FTS study by Keppler et al. [13] and the FTS studies of Refs. [3,14-17,30-32], limited to the strongest bands.

Although having frequently incomplete rotational structure, 32 bands of the main isotopologue are newly reported. The experimental positions and intensities are provided for each band in the **Supplementary Material I.** The upper panel of **Fig. 3** shows an overview of the assigned transitions. It is interesting to note that the $\nu_2+2\nu_3$ band of $^{12}C_2HD$ near 6932 cm^{-1} falls in the spectral interval of smallest absorption and represents a significant fraction of the absorption in this region. In other words, the residual absorption is this region depends on the acetylene D/H isotopic abundance. This situation is very similar to that encountered in the center of the 1.58 µm window of methane where the $3\nu_2$ band of CH_3D (normal relative abundance in methane of about 6×10^{-4}) contributes importantly to the absorption [33-36]. In the case of methane, this observation was found important for planetary applications as the $3\nu_2$ band of CH_3D was used to determine the D/H isotopic abundance in various the atmosphere of Titan [37,38], Uranus [39] and Neptune [40].

Note that about 3000 generally weak lines remain unassigned. We could not identify other impurities than water, carbon dioxide and methane (ethylene was also checked). Assuming that the $^{12}C^{13}CH_2$ and $^{12}C_2HD$ position lists of Refs [28,29] obtained with highly enriched samples are sufficiently complete to assign all the lines of these species in our spectra of natural acetylene, the remaining unassigned lines are thus believed to belong to the main isotopologue, $^{12}C_2H_2$.

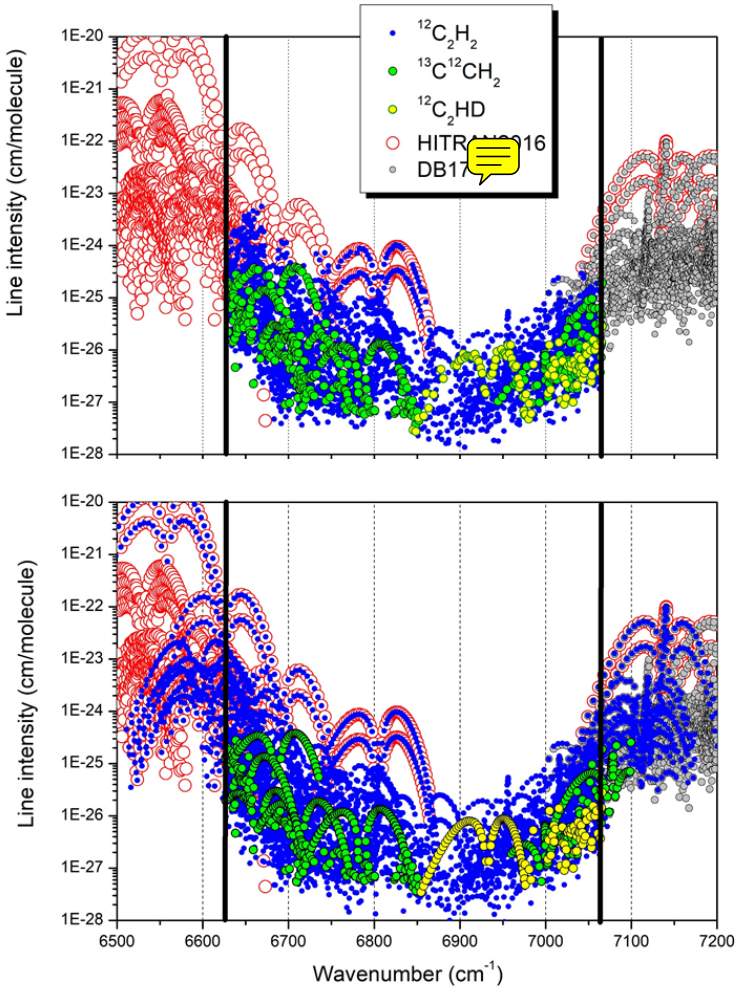

Fig. 3
Different line lists for acetylene in the 6500-7200 cm^{-1} region, including the 6627-7065 cm^{-1} range presently investigated. [1] Both panels show the HITRAN2016 list [1] and our 2017 empirical database [2] (red open circles and grey disks, respectively). Transitions of $^{12}C_2H_2$, $^{12}C^{13}CH_2$ and $^{12}C_2HD$ measured in this work are plotted on the upper panel (blue, green and yellow, respectively). The lower panel shows the recommended line list constructed in this work with line parameters mostly calculated from the derived spectroscopic parameters and Herman-Wallis coefficients (see Text).

4. Line positions- Band-by-band analysis.

The rotational structure of every vibrational band was analysed using the standard formula for the rovibrational energy levels of an isolated vibrational state:

$$T(v, J, e/f) = G_{e/f} + B_{e/f}J(J+1) - D_{e/f}[J(J+1)]^2 + H_{e/f}[J(J+1)]^3 \quad (1)$$

where $G_{e/f}$ is the vibrational term value and $B_{e/f}$, $D_{e/f}$, and $H_{e/f}$ are the rotational and distortion constants of the *e* and *f* sub levels.

In the case of the principal isotopologue, the parameters of the lower vibrational levels were constrained to their fitted values of Refs. [7,10], except for the 0001210 and 00012-12 levels ($v_1v_2v_3v_4v_5l_4l_5\varepsilon$ notation). The spectroscopic constants of these two levels were determined from a fit of the line positions of the $(\nu_4+2\nu_5)^1$I - ν_5^1 and $(\nu_4+2\nu_5)^1$II - ν_5^1 bands reported in Ref. [41]. The lower vibrational levels spectroscopic constants of the $^{12}C^{13}CH_2$ and C_2HD isotopologues were taken from

Ref. [42] and Ref. [29], respectively. All lower level constants are included in **Table 2**. As the *e* and *f* sub-bands may be perturbed in a different way, different sets of spectroscopic parameters were fitted for the *e* and *f* levels. When a given sublevel was observed from different lower levels, its spectroscopic parameters were obtained from a simultaneous fit of the line positions of the different sub-bands. The results of the fit are provided for each band in the **Supplementary Material I.** The retrieved constants of the upper states are listed in **Table 2**.

Many bands centered outside the studied interval have high *J* transitions newly assigned in our region. This is in particular the case for the strong bands included in the HITRAN and EDB17 databases, below 6600 cm^{-1} and above 7050 cm^{-1}, respectively. For instance, the rotational structure of the bands provided by the HITRAN database was generally extended by 5 to high *J* values of the angular moment quantum number. In order to determine the corresponding spectroscopic constants, the set of wavenumbers used as input data of the fit combines the present CRDS values with HITRAN and EDB17 position values. The comparison of the upper and lower panels of **Fig. 3** allows one to identify the bands for which the CRDS data were extended with HITRAN and EDB17 line positions. The corresponding fits are marked "+H" and "+EDB17" in the last column of **Table 2** and the source of each line is indicated in the **Supplementary Material I**. Note that for a number of strong lines with intensity larger than 10^{-24} cm/molecule, the absorption was too strong to allow for an accurate line center determination from the recorded CRDS spectra. In those situations, the HITRAN and EDB17 values were adopted, too (see **Fig. 3)**.

Part of the observed bands are rotationally perturbed (they are marked with "P" in **Table 2**). Some perturbations may result in anomalously large or negative values of the distortion constants. In the cases where the perturbation does not allow reproducing the rotational structure using Eq. (1), the fit was limited to the low rotational quantum numbers. After exclusion of the lines with poorly determined centers or affected by perturbation (see column n_{fit}/N_{tot} in **Table 2**), the average *rms* values of the (meas.-fit) differences are on the order of 2×10^{-3} cm^{-1} which is close to our claimed accuracy on the measured line positions.

In the first column of **Table 2**, we provide the $(v_1v_2v_3v_4v_5l_4l_5\varepsilon)$ normal mode labeling and symmetry type (*e* or *f*) relative to the Wang transformation. The vibrational labeling is obtained from the global effective Hamiltonian [24] and usually corresponds to the maximum fraction of the low *J* eigenfunctions in the normal mode basis. When different states have identical dominant normal mode contribution, in order to avoid duplicate vibrational labeling, we chose one of the major contributors to differentiate the states. For instance, the states at 7015.94 and at 7051.01 cm^{-1} have the same major contribution (020412-1) and important contributions from 0113010 and 0204101 basic functions. After analyzing the mixing scheme, it has been decided to attribute the 0113010 and 0204101 labeling to the state at 7051.01 and 7054.34 cm^{-1}, respectively. The vibrational notation of Plíva adopted in the HITRAN database is also provided in **Table 2**: $v_1v_2v_3(v_4v_5)^{\ell_t}r$ with $\ell=\left|\ \ell_4+\ell_5\ \right|$, ℓ_t being the vibrational angular momentum quantum number associated with the degenerated bending mode *t*, ± being the

symmetry type for Σ vibrational states (l= 0), and r a roman numeral indicating the rank of the level, by decreasing energy value (r= I for the highest energy level), inside the set of states having the same ℓ value.

The dipole transitions with $|\Delta K|>1$ are observed only as a result of vibration-rotation interaction. Unexpectedly, thanks to the high sensibility of the CRDS technique, the highly forbidden $H_u - \Sigma_g^+$ $2\nu_2+(4\nu_4+\nu_5)^5$ band corresponding to ΔK= 5 is detected near 7052.15 cm^{-1} (line intensities are smaller than 4×10^{-26} cm/molecule). The identification of this ΔK= 5 band was made possible because it is well predicted in the ASD.

In the case of the $2\nu_3+\nu_4^1$ band of the $^{12}C^{13}CH_2$ isotopologue, the set of positions used for the fit of the spectroscopic parameters was obtained by gathering the present CRDS values and the FTS line positions reported in Ref. [3] (mark "+FTS15") below and above 7065 cm^{-1}, respectively. The position fit revealed that the upper vibrational states of the $^{12}C^{13}CH_2$ bands reported in Ref. [28] as $2\nu_1+\nu_5^1-\nu_5^1$ and $2\nu_1+\nu_5^1-\nu_4^1$ are close (7393.02 and 7394.17 cm^{-1}, respectively) but cannot be the same. A note has been added in **Table 1** to indicate the ambiguity of the upper state labeling of these two $^{12}C^{13}CH_2$ levels.

5. Line intensities.

The rotational intensity distribution of a given vibrational band was modelled deriving the vibrational transition dipole moment squared and Herman-Wallis (HW) coefficients. The intensity, $S_{V'J'\varepsilon'\leftarrow VJ\varepsilon}$ (in cm/molecule), of a transition between two $VJ\varepsilon$ states defined (V and J are the vibrational index and the angular momentum quantum number, respectively; ε= ± is the parity), at a temperature T (in K) is related to the transition dipole moment squared, $|R|^2$:

$$S_{V'J'\varepsilon'\leftarrow VJ\varepsilon}(T)=\frac{8\pi^3}{3hc}Cg_{VJ\varepsilon}\frac{\nu_{V'J'\varepsilon'\leftarrow VJ\varepsilon}}{Q(T)}\exp\left(-\frac{hcE_{VJ\varepsilon}}{kT}\right)\left[1-\exp\left(-\frac{hc\nu_{V'J'\varepsilon'\leftarrow VJ\varepsilon}}{kT}\right)\right]L(J,K)\left|R\right|^2 \quad (2)$$

where $E_{VJ\varepsilon}$ is the lower state energy and $\nu_{V'J'\varepsilon'\leftarrow VJ\varepsilon}$ is the transition wavenumber, $Q(T)$ is the total internal partition function at temperature T, C is the isotopic abundance, $g_{VJ\varepsilon}$ is the nuclear statistical weight of the lower state and $L(J,K)$ is the Hönl-London factor. The values of the total internal partition functions of $^{12}C_2H_2$, $^{12}C^{13}CH_2$ and C_2HD at 296K and their natural isotopic abundances were taken from HITRAN database (https://hitran.org/docs/iso-meta/).

The expression of the Hönl-London factors for parallel (ΔK= 0), perpendicular (ΔK = ±1) and ΔK = ±2 forbidden bands can be found in Ref. [2] (the ΔK >2 bands were found too perturbed to have their intensities fitted). To reduce the data, $|R|^2$ is expanded empirically to take account for the rotational dependence:

$$|R|^2 = |R_0|^2\,(1 + A_1^{RP}\,m + A_2^{RP}\,m^2)^2 \text{ (P- and R-branches)}, \quad (3)$$

$$|R|^2 = |R_0|^2\,(1 + A_2^{Q}\,m^2)^2 \text{ (Q-branch)}, \quad (4)$$

m being equal to –*J* in the *P*-branch, *J*+1 in the *R*-branch, and *J* in the *Q*-branch. $|R_0|^2$ is the vibrational transition dipole moment squared and A_1^{RP}, A_2^{RP}, and A_2^{Q} are the Herman-Wallis coefficients. Note that we use the squared form of the terms between parentheses in Eqs. (3,4) accordingly to our previous publication [2].

The above empirical modeling of the intensity distribution was possible only for part of the observed bands because, for a significant number of them, important intensity perturbation or too scarce intensity information hinder a satisfactory fit of the measured intensities. The fitted values of the vibrational transition dipole moments squared and Herman-Wallis coefficients obtained from an unweighted fit of the experimental intensity values are given in **Table 3** for 47 bands. These bands are marked with "HW" in the first column of **Table 2.** The results of the fits including calculated line intensities and the relative differences from their measured values are provided in **Supplementary Material 2**. As a result of the frequent line overlapping and of the weakness of many bands, a significant number of line intensities are not sufficiently accurate and were excluded from the fit. Very often, different sublevels of a given band could not be fitted with the same set of empirical parameters. Assuming that it is due to different perturbation mechanisms, we provide in these cases different sets of empirical parameters for each-sub band. Considering the root mean square deviation of the intensity fit, given in **Table 3** for every band, we estimate the accuracy of the calculated line intensities to be about 10%.

6. Recommended empirical line list and comparison to HITRAN and ASD databases

6.1 Recommended list

The recommended line list is provided as **Supplementary Material 3** with a tag for each line indicating the origin of its position and intensity values. Overall, the final list, presented on the lower panel of **Fig. 3**, contains 4555 lines of $^{12}C_2H_2$, 591 lines of $^{12}C^{13}CH_2$ and 114 lines of C_2HD. For the 47 bands with intensity modeling listed in **Table 3** line parameters were calculated following the same procedure as used in Ref. [2]. In absence of perturbation, line positions were calculated using the spectroscopic parameters of **Table 2**. Line intensities were computed using the $|R_0|^2$ and Herman-Wallis coefficients of **Table 3.** For each branch of a given band, the line positions and line intensities were calculated for all the transitions up to a maximum *J* value exceeding by 1 the largest *J* value of the observations in the considered branch. Such an approach allows smoothing the measurement errors, completing the experimental line list by interpolation and extending moderately beyond the observations. Note that some of these 47 bands include a few lines with perturbed positions. In such cases (about 220 in total), we kept in the recommended line list the measured line positions but intensity values are calculated. These 47 bands include all the dominant bands and correspond to more than 3000 transitions bringing more than 99% of the absorption in the region. Nevertheless, for a large amount of weak or super weak bands (76 in total), the spectroscopic parameters could be fitted but the empirical modeling of the line intensities was not possible. In those cases, the lines - about 2000 in

total - were incorporated in the recommended list with measured values for both the position and the intensity.

The number of lines is given for each band in **Table 3** together with the maximum *J* quantum number for each branch. Note, that for completeness, we give in the recommended line list the whole rotational structure of all bands contributing to the studied region thus including transitions below and above the 6627-7065 cm^{-1} studied interval (see **Fig. 3**).

6.2 Comparison with the Acetylene Spectroscopy Databank (ASD)

The comparison with the ASD is illustrated in **Fig. 4** which includes a superposition of the ASD list and of our recommended list of $^{12}C_2H_2$, the corresponding differences of the position values and the ratios of the ASD and recommended intensities *versus* the transition wavenumbers. The bands corresponding to the ΔP= 10 and ΔP= 11 series can be distinguished (orange and blue symbols, respectively).

The ASD [25] is based on the global modeling for both line positions and line intensities of $^{12}C_2H_2$, using the effective operators approach presented in Ref. [24], in the 50–9900 cm^{-1} region. 237 fitted effective Hamiltonian parameters allowed reproducing 24,991 measured line positions of 494 bands with an *rms* deviation of 3.7×10^{-3} cm^{-1}. Although a significant fraction of the (ASD-measured) position differences exceeds this *rms* value, most of the position differences do not exceed 0.05 cm^{-1}. Note that part of the CRDS line positions reported by Robert et al. [18] and Amyay et al. [19] in our region were used as input data of the fit of the EH parameters used for ASD. Nevertheless, a large fraction of these CRDS line positions could not be satisfactorily accounted by the EH and were thus excluded. For instance, over a total of 1542 positions reported in Ref. [19], 437 were excluded from the fit and an *rms* deviation of 12.1×10^{-3} cm^{-1}, largely above the global *rms*~~, was~~ obtained. A very similar situation was encountered in our recent analysis of the acetylene spectrum in 5693–5882 cm^{-1} region [10]. This situation, confirmed by the present work, seems to indicate that the global EH of Ref. [24] is not fully adequate to account for the high sensitivity spectrum in the two regions.

More serious disagreements are noted for line intensities. Very large overestimations of ASD intensities are found for a number of bands, in particular in the ΔP= 10 series. The ASD intensities of the $\nu_1+\nu_3+2\nu_5^0-2\nu_4^0$ band are about four orders of magnitude larger than measured (out of scale in **Fig. 4**). The measured intensities of the $\nu_1+\nu_2+(\nu_4+3\nu_5)^0-2\nu_4^0$, $2\nu_1+(\nu_4+\nu_5)^0-2\nu_4^0$ and $2\nu_1+(\nu_4+2\nu_5)^1II-(2\nu_4+\nu_5)^1I$ hot bands are also overestimated by about two orders of magnitude. As mentioned above, the ΔP= 10 and ΔP= 11 EDM parameters used for the ASD were determined from a fit of the FTS intensity values of the strongest bands (see Table 7 of Ref. [24]). The observed large overestimation of the ASD predicted band intensities for a series of weak hot band remains to be explained. Indeed, in case of newly detected bands, the most frequent situation is an underestimation of the ASD predicted intensities due to missing EDM terms (see for instance Ref. [12]). Important improvements of the ΔP=

10 and ΔP= 11 EDM parameters is thus expected res[illegible]rom the inclusion of the large set of experimental data obtained in this work.

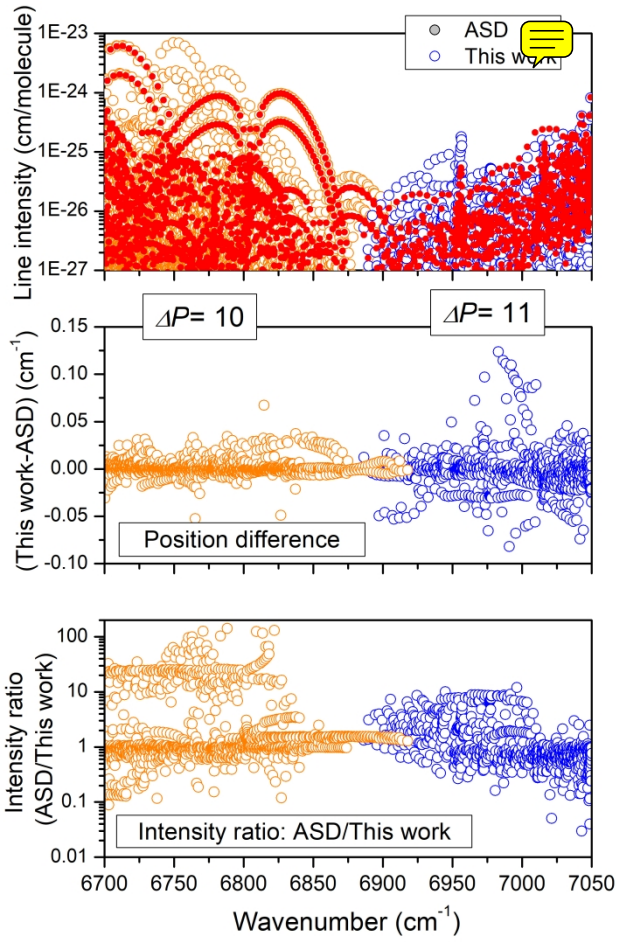

Fig. 4.
Comparison of the acetylene spectroscopy databank (ASD) to our recommended list for $^{12}C_2H_2$. The bands corresponding to the ΔP= 10 and ΔP= 11 series are plotted with orange and blue symbols, respectively.

6.3 Comparison with the HITRAN2016 database

As illustrated by the overview comparison presented in **Fig. 5,** the HITRAN2016 list is limited to the strongest ΔP= 10 bands in our region and ΔP= 11 bands are practically absent (see **Fig. 1**). The HITRAN2016 list of acetylene was elaborated by Jacquemart et al. as described in Ref. [14]. In our region, the HITRAN positions are FTS values reported by Keppler et al. [13] except for the $\nu_1+\nu_2+(\nu_4+\nu_5)^0$ band at 6623.13 cm^{-1} for which Ref. [15] was chosen as source. HITRAN line positions show a number of important deviations compared to our values, up to 0.44 cm^{-1} for the high J lines of the band centered at 6616.57 cm^{-1} (This band has a different vibrational labeling in HITRAN and in our list, is 102111u-000101g and 02023 2-1 00010 1 0, respectively). We have included on the middle panel of **Fig. 5**, the deviations between our recommended line positions and the original FTS values reported in Keppler et al. The obtained agreement is very good and the plot clearly indicates

that the discrepancies are due to hazardous high *J* extrapolations of Ref. [14]. In fact, for a number of high *J* and some low *J* transitions included in HITRAN2016, lower state combination difference relations are not fulfilled. This ~~is~~ might be due to the mixing of measured line centers from Keppler et al. with line centers calculated with empirical spectroscopic parameters in Ref. [14]. No doubt that our present list will help to correct these issues.

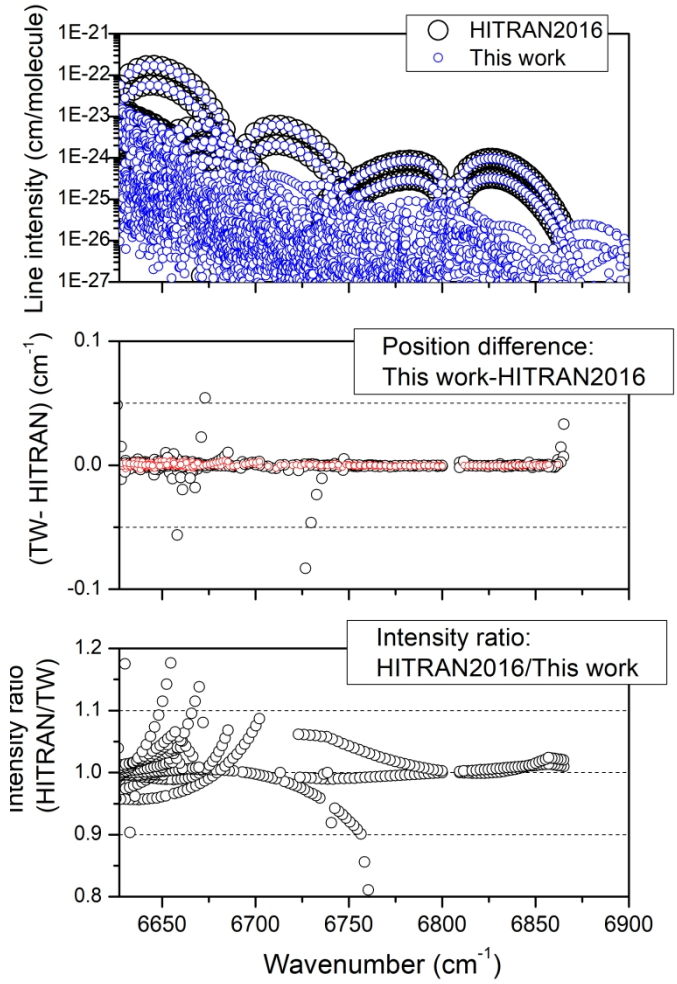

Fig. 5.
Comparison of the HITRAN line list to our recommended list for $^{12}C_2H_2$ (black and blue symbols on the upper panel, respectively). On the middle panel, the differences between our values and the FTS values of Keppler et al. [13] (red circles) are superimposed to the deviations between our values and HITRAN values (black circles).

According to Ref. [14], HITRAN intensities in the region were calculated using the vibrational transition dipole moment squared and Herman-Wallis coefficients derived from FTS measurements in Refs. [15-17]. Although an agreement within about 10 % is observed for most of the lines, very large overestimations (up to a factor 170!) are noted. The largest discrepancies concern the above mentioned band centered at 6616.57 cm^{-1} and are probably related to similar extrapolation issues as for line positions, the sensitivity of the FTS spectra of Refs. [15-17] being about three orders of magnitude lower than the sensitivity of the present CRDS spectra.

7. Concluding remarks

The high sensitivity absorption spectrum of acetylene has been analyzed by CRDS in the 1.45 μm window (6627-7065 cm^{-1}). Compared to the previous CRDS investigations [18,19], the set of rovibrational assignments has been roughly duplicated. Of importance for applications and inclusion in spectroscopic databases, detailed intensity information is provided for the first time. In total about 3600 lines were assigned to 123 bands of the $^{12}C_2H_2$, $^{12}C^{13}CH_2$ and $^{12}C_2HD$ isotopologues present in natural abundance in the acetylene sample. The weakest lines have an intensity of a few 10^{-28} cm/molecule at 296 K. The detection of about one hundred transitions of the $^{12}C_2HD$ minor isotopologue (relative abundance of about 3×10^{-4}) illustrates the sensitivity of the recordings. Interestingly, the $\nu_2+2\nu_3$ of $^{12}C_2HD$ has a significant contribution to the absorption near 6900 cm^{-1} corresponding to the most transparent interval of the considered acetylene window.

Using spectroscopic parameters derived for all upper vibrational levels, vibrational transition dipole moment squared and Herman-Wallis coefficients derived for 47 bands and literature data for a few strong lines a recommended list of more than 5000 transitions was generated in the region.

The current HITRAN2016 database provides spectral information for only ten bands in the 6627-7066 cm^{-1} region under study. The comparison with our recommended line list revealed some strong discrepancies concerning transitions extrapolated beyond the positions reported by Keppler et al. or beyond the intensity measurements of Refs. [15-17]. For the band centered at 6616.57 cm^{-1}, labeled 102111u-000101g in HITRAN notation, position differences reach values up to 0.44 cm^{-1} and some line intensities are strongly overestimated (up to a factor 170).

The ASD list based on a global empirical modeling of measured line positions and line intensities available in the literature has the advantage to be much more complete and to provide predicted line parameters which were highly valuable in the assignment process of our data. Nevertheless, in the investigated region, the effective Hamiltonian [24] used to generate the ASD cannot reproduce the observation within the experimental accuracy and a significant number of ASD transitions have ~~a~~ predicted line centers deviating by more than 0.01 cm^{-1} from the observations. As concerned line intensities, an important issue was evidenced for a number of ΔP= 10 hot bands which show ASD intensities exceeding the measured values by two to four orders of magnitude. The intensity information reported here will help to correct the set of dipole moment parameters of the ΔP= 10 series of bands.

Together with the recent CRDS study in the 5693-5882 cm^{-1} region [10] and a FTS study in the 9280-10740 cm^{-1} interval [11,12], the present results will allow to complete and extend our empirical database for acetylene between 5693 and 10740 cm^{-1} [2].

Acknowledgements

The supports of the CNRS (France) in the frame of International Research Project SAMIA are acknowledged with IAO Tomsk. O.L thanks Université Grenoble Alpes for a two-months support at LIPhy. This work was performed in the frame of the ANR project e_PYTHEAS (ANR-16-CE31-0005).

References

1. Gordon IE, Rothman LS, Hill C, Kochanov RV, Tan Y, Bernath PF, et al. The HITRAN2016 molecular spectroscopic database. J Quant Spectrosc Radiat Transfer 2017;203:3-69. https://doi.org/10.1016/j.jqsrt.2017.06.038
2. Lyulin O.M., Campargue A. An empirical spectroscopic database for acetylene in the regions of 5850-6341 cm^{-1} and 7000-9415 cm^{-1}. J Quant Spectrosc Radiat Transf 2017;203:461–471. 10.1016/j.jqsrt.2017.01.036
3. Lyulin OM, Vander Auwera J, Campargue A. The Fourier transform absorption spectrum of acetylene between 7000 and 7500 cm^{-1}. J Quant Spectrosc Radiat Transf 2015;160:85–93.
4. Lyulin OM, Vander Auwera J, Campargue A, The Fourier transform absorption spectrum of acetylene between 8280 and 8700 cm^{-1}. J Quant Spectrosc Radiat Transf 2016;177:234–240 http://dx.doi.org/10.1016/j.jqsrt.2015.11.026
5. Béguier S, Lyulin OM, Hu SM, Campargue A. Line intensity measurements for acetylene between 8980 and 9420 cm^{-1} J Quant Spectrosc Radiat Transf 2017;189:417-420. 10.1016/j.jqsrt.2016.12.020
6. Lyulin OM, Campargue A, Mondelain D, Kassi S. The absorption spectrum of acetylene by CRDS between 7244 and 7918 cm^{-1} J Quant Spectrosc Radiat Transf 2013;130:327–43.
7. Lyulin OM, Mondelain D, Béguier S, Kassi S, Vander Auwera J, Campargue A. High sensitivity absorption spectroscopy of acetylene by CRDS between 5851 and 6341 cm^{-1}. Mol Phys 2014;112:2433–44.
8. Kassi S, Lyulin OM, Béguier S, Campargue A. New assignments and a rare peculiarity in the high sensitivity CRDS spectrum of acetylene near 8000 cm^{-1}. J Mol Spectrosc 2016;326:106-114.
9. Jacquinet-Husson N, Armante R, Crépeau N, Chédin A, Scott NA, Boutammine C, et al. The 2015 edition of the GEISA spectroscopic database. J Mol Spectrosc 2016;327:31–72. doi:10.1016/j.jms.2016.06.007
10. Lyulin O.M., Vasilchenko S., Mondelain D., Campargue A., The CRDS spectrum of acetylene near 1.73 µm. J Quant Spectrosc Radiat Transf 2019;234:147-158. doi.org/10.1016/j.jqsrt.2019.04.006
11. Lyulin OM, Béguier S, Hu SM, Campargue A, The absorption spectrum of acetylene near 1 µm (9280–10740 cm^{-1}) (I): Line positions. J Quant SpectroscRadiatTransf 2018;208:179-187 DOI: 10.1016/j.jqsrt.2018.01.007
12. Lyulin OM, Campargue A. The absorption spectrum of acetylene near 1 µm (9280–10740 cm^{-1}) (II): Line intensities. J Quant Spectrosc Radiat Transf 2018;215:51-58. DOI: 10.1016/j.jqsrt.2018.04.025
13. Keppler KA, Mellau G, Klee S, Winnewisser BP, Winnewisser M, Pliva J, et al. Precision measurements of acetylene spectra at 1.4–1.7 µm recorded with 352.5-m pathlength. J Mol Spectrosc 1996;175:411-20.
14. Jacquemart D, Lacome N, Mandin JY, Dana V, Tran H, Gueye FK, et al. The IR spectrum of $^{12}C_2H_2$: line intensity measurements in the 1.4-µm region and update of the databases. J Quant Spectrosc Radiat Transf 2009;110:717–32.
15. El Hachtouki R. and Vander Auwera J. Absolute line intensities in acetylene: The 1.5 µm region. J Mol Spectrosc 2002;216:355-62
16. Tran H, Mandin JY, Dana V, Régalia-Jarlot L, Thomas X, Von der Heyden P. Line intensities in the 1.5-mm spectral region of acetylene. J Quant Spectrosc Radiat Transf 2007;108:342–62.
17. Lyulin OM, Perevalov VI, Tran H, Mandin JY, Dana V, Régalia-Jarlot L et al. Line intensities of acetylene: new measurements in the 1.5-µm spectral region and global approach in the ΔP= 10 series. J Quant Spectrosc Radiat Transf 2009;110:1815-24
18. Robert S, Herman M, Fayt A, Campargue A, Kassi S, Liu A, et al. Acetylene, $^{12}C_2H_2$: new CRDS data and global vibration-rotation analysis up to 8600 cm^{-1}. Mol Phys 2008;106:2581–605.
19. Amyay B, Herman M, Fayt A, Campargue A, Kassi S. Acetylene, $^{12}C_2H_2$: refined analysis of CRDS spectra around 1.52 µm. J Mol Spectrosc 2011;267:80–91.
20. Herman M, Liévin J, Vander Auwera J, Campargue C. Global and accurate vibration hamiltonians from high-resolution molecular spectroscopy. Adv Chem Phys 1999;108:1–431. Wiley, New York.
21. Herman M, Campargue C, El Idrissi MI, Vander Auwera J. Vibrational spectroscopic database on acetylene, $\tilde{X}^1\Sigma_g^+$ ($^{12}C_2H_2$, $^{12}C_2D_2$ and $^{13}C_2H_2$) J Phys Chem Ref Data 2003;32:921–1361.
22. Fayt A, Robert S, Di Lonardo G, Fusina L, Tamassia F, Herman M. Vibration-rotation energy pattern in acetylene: $^{12}CH^{12}CH$ up to 6750 cm^{-1} J Chem Phys 2007;126:114303/1–8..
23. Campargue A; Temsamani MA; Herman M. The absorption spectrum of C_2H_2 between 12800 and 18000 cm^{-1}: I. Vibrational assignments. Molecular Physics 1997;90:793–805.
24. Lyulin OM, Perevalov VI. Global modelling of vibration-rotation spectra of acetylene molecule. J Quant Spectrosc Radiat Transf 2016;177:59–74.
25. Lyulin O.M., Perevalov V.I. ASD-1000: High-resolution, high-temperature acetylene spectroscopic databank. J Quant Spectrosc Radiat Transf 2017;201:94–103.

26. Kassi S, Campargue A. Cavity ring down spectroscopy with 5×10^{-13} cm^{-1} sensitivity. J Chem Phys 2012;137:234201. doi: 10.1063/1.4769974
27. Macko P, Romanini D, Mikhailenko SN, Naumenko OV, Kassi S, Jenouvrier A et al. High sensitivity CW-cavity ring down spectroscopy of water in the region of the 1.5 μm atmospheric window. J Mol Spectrosc 2004;227:90-108. doi: 10.1016/j.jms.2004.05.020
28. Robert S., Amyay B., Fayt A., Di Lonardo G., Fusina L., Tamassia F., and Herman M. Vibration - Rotation Energy Pattern in Acetylene: $^{13}CH^{12}CH$ up to 10120 cm^{-1}. J. Phys. Chem. A 2009; 113:13251–13259.
29. Liévin J., Abbouti Temsamani M., Gaspard P., Herman M. Overtone spectroscopy and dynamics in monodeuteroacetylene (C2HD). Chemical Physics 1995;190:419-445.
30. Kou Q, Guelachvili G, Abbouti Temsamani M, Herman M. The absorption spectrum of C_2H_2 around $\nu_1+\nu_3$: energy standards in the 1.5μm region and vibrational clustering. Can J Phys 1994;72:1241–50.
31. Henningsen J, Sørensen GO. On modeling the overtone bands of acetylene in the 1500 nm region. Abstracts of the Seventeenth Colloquium on High Resolution Molecular Spectroscopy. University of Nijmegen, 9–13 September 2001, poster L17. p. 267.
32. Vander Auwera J, El Hachtouki, Brown L. Absolute line wave-numbers in the near infrared: $^{12}C_2H_2$ and $^{12}C^{16}O_2$. Mol Phys 2002;100:3563–76.
33. Lutz BL, de Bergh C, Maillard JP. Monodeuterated methane in the outer solar system. I. Spectroscopic analysis of the bands at 1.55 and 1.95 microns. Astrophys J 1983;273:397-409.
34. Wang L, Kassi S, Liu AW, Hu SM, Campargue A. High sensitivity absorption spectroscopy of methane at 80 K in the 1.58 μm transparency window: Temperature dependence and importance of the CH_3D contribution. J Mol Spectrosc 2010;261:41-52.
35. Lu Y, Mondelain D, Kassi S, Campargue A. The CH_3D absorption spectrum in the 1.58 μm transparency window of methane: empirical line lists and temperature dependence between 80 K and 296 K. J Quant Spectrosc Radiat Transfer 2011;112:2683-97.
36. Campargue A, Wang L, Kassi S, Mondelain D, Bézard B, Lellouch E, Coustenis A, de Bergh C, Hirtzig M, Drossart P. An empirical line list for methane in the 1.26-1.71 μm region for planetary investigations (T= 80-300 K). Application to Titan. Icarus 2012;219:110-28.
37. De Bergh C, Lutz BL, Owen T, Chauville J. Monodeuterated methane in the outer solar system. III. Its abundance on Titan. Astrophys J 1988;329:951-55.
38. Penteado PF, Griffith CA, Greathouse TK, de Bergh C. Measurements of CH_3D and CH_4 in Titan from infrared spectroscopy. Astrophys J 2005;629:L53-L56
39. De Bergh C, Lutz BL, Owen T, Brault J, Chauville J. Monodeuterated methane in the outer solar system. II. Its detection on Uranus at 1.6 microns. Astrophys J 1986;311:501-10.
40. De Bergh C, Lutz BL, Owen T, Maillard JP. Monodeuterated methane in the outer solar system. IV. Its detection and abundance on Neptune. Astrophys J 1990;355:661-666.
41. Kabbadj Y., Herman M., Di Lonardo G., Fusina L., and Johns J. W. C., The bending energy levels of C_2H_2 J. Mol. Spectrosc. 1991;150:535-565.
42. Cané E., Fusina L., Tamassia F., Fayt A., Herman M., Robert S., Vander Auwera J., The FT absorption spectrum of $^{13}CH^{12}CH$: rotational analysis of the vibrational states from 3800 to 6750 cm^{-1}. Molecular Physics 2006:104:515–526.

Table 1. Spectroscopic parameters (in cm^{-1}) of the rovibrational bands of $^{12}C_2H_2$, $^{13}C^{12}CH_2$ and C_2HD assigned in the CRDS spectra of acetylene between 6627 and 7066 cm^{-1}. The bands are listed according to increasing values of the upper state energy levels.

$v_1v_2v_3v_4v_5l_4l_5\varepsilon^a$	G_c	$B_{e/f}$	$D_{e/f}\times10^6$	$H_{e/f}\times10^{10}$	$n_{fit}/N_{tot}{}^b$	Bands[c]	*Band type*	ΔG_c[d]	*observed lines*[e]	*rms*[f]	Previous reports[g]
0000000	0.0	1.1766462	1.6270	0.016							
0001010f	611.693755	1.18055377	1.67973	0.0187							
0001010e	611.693759	1.17532307	1.6405	0.0177							
0000101e	729.15410	1.1764413	1.6326	0.017							
0000101f	729.15410	1.1811398	1.6714	0.018							
0002020f	1228.7997	1.179109	1.692								
0002020e	1228.8011	1.17908	19.0	245							
0002000	1230.3894	1.17937	-15.8	-246							
000111-1e	1328.0722	1.180508	3.595	2.76							
000111-1f	1340.5507	1.1800836	1.715								
0001111f	1342.8023	1.179838	1.647								
0001111e	1342.8034	1.179804	-0.226	-2.78							
0000200	1449.1107	1.181234	4.415	6.52							
0000202f	1458.2936	1.180757	1.669								
0000202e	1458.2944	1.180714	-1.052	-6.43							
0003030e	1851.3699	1.180358	10.15								
0003030f	1851.3749	1.18006	6.33	39							
0003010f	1854.5970	1.18583	-3.8	-61							
0003010e	1854.5978	1.17533	-6.2								
0002121f	1961.9321	1.180731	-1.03	-5.15							
0002121e	1961.9332	1.18069	-1.31	-10							
0001212e	2074.175	1.181594	1.113								
0001212f	2074.1826	1.181497	0.80								
0000301f	2169.1559	1.188211	2.782	-1.89							
0000301e	2169.1575	1.178631	2.55	1.65							
0001210f	2047.8761(4)	1.187537(3)	2.592(6)	-1.48(3)	70/71	$(\nu_4+2\nu_5)^1\Pi - \nu_5^1$	$\Pi_g - \Pi_u$	1318.7220(4)	P37/R37	1.4	
0001210e	2047.8766(4)	1.177928(3)	2.457(6)	1.13(3)	63/65	$(\nu_4+2\nu_5)^1\Pi - \nu_5^1$	$\Pi_g - \Pi_u$	1318.7225(4)	P36/R36	0.7	
00012-12f	2065.7923(4)	1.184239(3)	1.672(3)		41/45	$(\nu_4+2\nu_5)^1\Pi - \nu_5^1$	$\Pi_g - \Pi_u$	1336.6382(4)	P20/R27	1.4	
00012-12e	2065.7929(4)	1.180042(3)	1.618(4)		44/49	$(\nu_4+2\nu_5)^1\Pi - \nu_5^1$	$\Pi_g - \Pi_u$	1336.6388(4)	P22/R28	1.5	
***P*=10**											
HW 10100 0 0e	6556.4648(5)	1.163777(2)	1.606(2)	0.022(6)	68/68	$\nu_1+\nu_3$	$\Sigma_u^+ - \Sigma_g^+$	6556.4648(5)	P21/R53	0.6	+H [15,16,30,31]

HW 11011 1-1e	6623.1363(5)	1.167978(4)	4.041(7)	4.21(3)	59/66	$\nu_1+\nu_2+(\nu_4+\nu_5)^0$	$\Sigma_u^+-\Sigma_g^+$	6623.1363(5)	P23/R47	1.3	+H [13,15,16,30,31]
11011 1 1e	6636.750(1)	1.167338(6)	-0.473(8)	-3.81(3)	34/35	$\nu_1+\nu_2+(\nu_4+\nu_5)^2$	$\Delta_u-\Sigma_g^+$	6636.750(1)	R4-43	2.5	[19]
HW 02013 1-1e	6654.2517(6)	1.171792(8)	8.18(2)	20.6(2)	49/54	$2\nu_2+(\nu_4+3\nu_5)^{0+}$	$\Sigma_u^+-\Sigma_g^+$	6654.2517(6)	P20/R33	1.6	+H [13,16,30]
02013-1 3e	6664.460(9)	1.17124(6)	-4.1(2)	-22(1)	11/12	$2\nu_2+(\nu_4+3\nu_5)^2$II	$\Delta_u-\Sigma_g^+$	6664.460(9)	R11-27	1.0	[19]
02013 1 1e	6686.975(2)	1.17129(2)	3.95(5)	-1.7(4)	22/37	$2\nu_2+(\nu_4+3\nu_5)^2$I	$\Delta_u-\Sigma_g^+$	6686.975(2)	P22/R41	2.4 **P**	[19]
HW 01102 0 0e	6690.5762(6)	1.16927(1)	2.23(4)	11.5(4)	46/64	$\nu_2+\nu_3+2\nu_5^0$	$\Sigma_u^+-\Sigma_g^+$	6690.5762(6)	P30/R33	1.6	+H [13,16,30]
01102 0 2e	6701.175(2)	1.168988(9)	-0.11(1)	-4.43(6)	17/33	$\nu_2+\nu_3+2\nu_5^2$	$\Delta_u-\Sigma_g^+$	6701.175(2)	P27/R39	1.9	[19]
02013 1 3e	6704.137(1)	1.169142(4)	-0.012(3)		17/23	$2\nu_2+(\nu_4+3\nu_5)^4$	$\Gamma_u-\Sigma_g^+$	6704.137(1)	P30/R37	2.8	[19]
***P*=11**											
HW 02041 2-1f	7015.936(2)	1.17819(2)	-0.24(6)	10(5)	21/21	$2\nu_2+(4\nu_4+\nu_5)^1$II	$\Pi_u-\Sigma_g^+$	7015.936(2)	Q28	1.8	[3,19]
HW 02041 2-1e	7015.9522(9)	1.16495(2)	-2.40(8)	11(1)	25/34	$2\nu_2+(4\nu_4+\nu_5)^1$II	$\Pi_u-\Sigma_g^+$	7015.9522(9)	P25/R13	2.0 **P**	[3,19]
01130 1 0e	7051.007(2)	1.17289(9)	5(1)	-203(30)	11/23	$\nu_2+\nu_3+3\nu_4^1$	$\Pi_u-\Sigma_g^+$	7051.007(2)	P25-3	1.5 **P**	+EDB17, [3,19]
01130 1 0f	7051.017(1)	1.16791(4)	-2.1(3)	-100(6)	14/17	$\nu_2+\nu_3+3\nu_4^1$	$\Pi_u-\Sigma_g^+$	7051.017(1)	Q18	2.3	+EDB17 ,[3]
02041 4 1e	7052.151(7)	1.16800(3)	1.22(3)		8/10	$2\nu_2+(4\nu_4+\nu_5)^5$	$H_u-\Sigma_g^+$	7052.151(7)	P29-17	2.0	
02041 4 1f	7052.554(5)	1.16515(2)	-1.78(3)		6/6	$2\nu_2+(4\nu_4+\nu_5)^5$	$H_u-\Sigma_g^+$	7052.554(5)	Q13-27	1.5	
02041 2 1f	7054.330(8)	1.17796(3)	1.02(2)		13/16	$2\nu_2+(4\nu_4+\nu_5)^3$I	$\Phi_u-\Sigma_g^+$	7054.330(8)	Q16-33	0.7	
02041 0 1f	7054.346(4)	1.1708(5)	36(10)	1312(460)	5/13	$2\nu_2+(4\nu_4+\nu_5)^1$I	$\Pi_u-\Sigma_g^+$	7054.346(4)	Q23	0.1 **P**	+EDB17,[3]
02041 0 1e	7054.353(3)	1.1651(2)	25(4)	1374(180)	14/19	$2\nu_2+(4\nu_4+\nu_5)^1$I	$\Pi_u-\Sigma_g^+$	7054.353(3)	P17/R9	2.3 **P**	+EDB17,[3]
02041 2 1e	7054.57(1)	1.1720(5)	-15(4)		5/21	$2\nu_2+(4\nu_4+\nu_5)^3$I	$\Phi_u-\Sigma_g^+$	7054.57(1)	P31-5	2.5 **P**	[19]
HW 10110 1 0f	7141.5028(6)	1.168113(3)	1.664(2)		36/38	$\nu_1+\nu_3+\nu_4^1$	$\Pi_u-\Sigma_g^+$	7141.5028(6)	Q39	1.0	+H [3,14,32]
HW 10110 1 0e	7141.5032(4)	1.162657(1)	1.6154(5)		76/79	$\nu_1+\nu_3+\nu_4^1$	$\Pi_u-\Sigma_g^+$	7141.5032(4)	P51/R35	1.1	+H [3,14,32]
HW 11021 2-1f	7205.9511(6)	1.174950(5)	3.42(1)	0.12(5)	62/72	$\nu_1+\nu_2+(2\nu_4+\nu_5)^1$II - ν_4^1	$\Pi_u-\Pi_g$	6594.2573(6)	P30/R44	1.5	+H [13,16,30]
HW 11021 2-1e	7205.9521(6)	1.164825(5)	2.780(8)	1.93(3)	56/69	$\nu_1+\nu_2+(2\nu_4+\nu_5)^1$II - ν_4^1	$\Pi_u-\Pi_g$	6594.2583(6)	P30/R42	2.0	+H [13,16,30]
HW 00201 0 1f	7218.1998(6)	1.168875(6)	2.07(1)	0.69(6)	49/57	$2\nu_3+\nu_5^1$ - ν_4^1	$\Pi_u-\Pi_g$	6606.5060(6)	P20/R41	1.0	+H [13,16,30]
HW 00201 0 1e	7218.2008(6)	1.166465(4)	2.580(8)	1.82(3)	64/69	$2\nu_3+\nu_5^1$ - ν_4^1	$\Pi_u-\Pi_g$	6606.5070(6)	P30/R42	1.5	+H [13,16,30]
HW 11021 2 1f	7228.065(1)	1.168278(8)	2.80(1)	2.96(5)	25/35	$\nu_1+\nu_2+(2\nu_4+\nu_5)^3$ - ν_4^1	$\Phi_u-\Pi_g$	6616.371(1)	R5-42	1.9 **P**	[19]
11021 2 1e	7228.079(3)	1.16784(6)	3.4(3)	16(4)	12/21	$\nu_1+\nu_2+(2\nu_4+\nu_5)^3$ - ν_4^1	$\Phi_u-\Pi_g$	6616.385(3)	R4-31	2.4 **P**	[19]
HW 02023 2-1e	7228.260(1)	1.16861(3)	-1.2(3)	-48(6)	31/52	$2\nu_2+(2\nu_4+3\nu_5)^1$III - ν_4^1	$\Pi_u-\Pi_g$	6616.566(1)	P25/R29	1.5 **P**	+H [13,17,30]*
HW 02023 2-1f	7228.278(1)	1.17232(2)	4.64(6)	24.3(6)	38/58	$2\nu_2+(2\nu_4+3\nu_5)^1$III - ν_4^1	$\Pi_u-\Pi_g$	6616.584(1)	P25/R36	1.8 **P**	+H [13,17,30]*
HW 11021 0 1f	7234.292(1)	1.17416(2)	-1.56(5)	-26.2	18/24	$\nu_1+\nu_2+(2\nu_4+\nu_5)^1$I - ν_4^1	$\Pi_u-\Pi_g$	6622.598(1)	R2-30	2.7 **P**	[19]
11021 0 1e	7234.309(2)	1.166520(6)	0.231(5)		9/12	$\nu_1+\nu_2+(2\nu_4+\nu_5)^1$I - ν_4^1	$\Pi_u-\Pi_g$	6622.615(2)	R2-33	2.7	[19]
02023 2 1f	7256.347(4)	1.17142(2)	-0.21(3)	-0.8(1)	18/21	$2\nu_2+(2\nu_4+3\nu_5)^3$II - ν_4^1	$\Phi_u-\Pi_g$	6644.653(4)	R9-37	2.9	[19]
HW 01112 1 0f	7273.7683(8)	1.175847(9)	2.86(2)		29/31	$\nu_2+\nu_3+(\nu_4+2\nu_5)^1$II - ν_4^1	$\Pi_u-\Pi_g$	6662.0745(8)	P13/Q1/R22	1.9	[18]
HW 01112 1 0e	7273.7713(7)	1.165408(7)	2.38(1)		30/31	$\nu_2+\nu_3+(\nu_4+2\nu_5)^1$II - ν_4^1	$\Pi_u-\Pi_g$	6662.0775(7)	P13/R24	1.4	[18]
HW 02023 0 1f	7278.474(1)	1.17309(1)	2.60(3)	-5.0(2)	23/26	$2\nu_2+(2\nu_4+3\nu_5)^1$I - ν_4^1	$\Pi_u-\Pi_g$	6666.780(1)	P10/R32	1.6	[19]

HW 02023 0 1e	7278.478(1)	1.171300(6)	1.932(7)		19/22	$2\nu_2+(2\nu_4+3\nu_5)^1I - \nu_4^1$	$\Pi_u - \Pi_g$	6666.784(1)	P12/R30	1.8	[19]
HW 01112-1 2f	7286.124(1)	1.16855(2)	0.88(5)		22/24	$\nu_2+\nu_3+(\nu_4+2\nu_5)^1I - \nu_4^1$	$\Pi_u - \Pi_g$	6674.430(1)	P18/Q1/R18	2.2	[18,19]
02023 0 3e	7286.443(2)	1.172034(6)	0.	-5.93(4)	17/22	$2\nu_2+(2\nu_4+3\nu_5)^3I - \nu_4^1$	$\Phi_u - \Pi_g$	6674.749(2)	R7-34	3.2	[19]
02023 0 3f	7286.510(3)	1.17140(2)	0.81(4)		8/9	$2\nu_2+(2\nu_4+3\nu_5)^3I - \nu_4^1$	$\Phi_u - \Pi_g$	6674.816(3)	R3-21	2.9	[19]
HW 11012 1 0e	7329.3396(6)	1.165198(6)	2.61(1)	1.57(8)	57/62	$\nu_1+\nu_2+(\nu_4+2\nu_5)^1II - \nu_5^1$	$\Pi_g - \Pi_u$	6600.1855(6)	P30/R34	1.3	+H [13,16,30]
HW 11012 1 0f	7329.3428(6)	1.175603(5)	2.944(9)	-1.03(4)	65/66	$\nu_1+\nu_2+(\nu_4+2\nu_5)^1II - \nu_5^1$	$\Pi_g - \Pi_u$	6600.1887(6)	P30/R39	1.8	+H [13,16,30]
HW 11012-1 2e	7350.139(1)	1.171555(7)	1.759(8)		19/24	$\nu_1+\nu_2+(\nu_4+2\nu_5)^1I - \nu_5^1$	$\Pi_g - \Pi_u$	6620.985(1)	R2-31	1.6	[19]
HW 11012-1 2f	7350.142(1)	1.167028(8)	1.68(1)		20/20	$\nu_1+\nu_2+(\nu_4+2\nu_5)^1I - \nu_5^1$	$\Pi_g - \Pi_u$	6620.988(1)	R3-27	1.3	[19]
11012 1 2e	7353.782(3)	1.16950(2)	1.33(2)		12/13	$\nu_1+\nu_2+(\nu_4+2\nu_5)^3 - \nu_5^1$	$\Phi_g - \Pi_u$	6624.628(3)	R2-27	2.8	[19]
11012 1 2f	7353.952(2)	1.168794(8)	0.392(5)		13/15	$\nu_1+\nu_2+(\nu_4+2\nu_5)^3 - \nu_5^1$	$\Phi_g - \Pi_u$	6624.798(2)	R4-36	3.0	[19]
HW 02014-1 2f	7362.732(3)	1.18083(3)	4.74(4)		6/7	$2\nu_2+(\nu_4+4\nu_5)^1II - \nu_5^1$	$\Pi_g - \Pi_u$	6633.578(3)	R6-23	1.4	
HW 02014-1 2e	7362.752(1)	1.16683(1)	3.15(2)		12/15	$2\nu_2+(\nu_4+4\nu_5)^1II - \nu_5^1$	$\Pi_g - \Pi_u$	6633.598(1)	R1-24	2.2	[19]
02014 1 0e	7394.327(2)	1.17694(4)	5.1(2)	-3.3(2)	12/27	$2\nu_2+(\nu_4+4\nu_5)^1I - \nu_5^1$	$\Pi_g - \Pi_u$	6665.173(2)	P10/R34	4.1 **P**	[19]
02014 1 0f	7394.329(6)	1.16962(8)	3.1(3)		8/9	$2\nu_2+(\nu_4+4\nu_5)^1I - \nu_5^1$	$\Pi_g - \Pi_u$	6665.175(6)	P9/R14	1.1	[19]
HW 01103 0 1e	7401.3826(8)	1.16748(2)	1.7(1)	50(2)	37/39	$\nu_2+\nu_3+3\nu_5^1 - \nu_5^1$	$\Pi_g - \Pi_u$	6672.2285(8)	P17/Q12/R20	1.1	[18,19]
HW 01103 0 1f	7401.3832(8)	1.17570(1)	2.18(4)	-10.4(4)	36/37	$\nu_2+\nu_3+3\nu_5^1 - \nu_5^1$	$\Pi_g - \Pi_u$	6672.2291(8)	P18/Q1/R26	1.6	[18,19]
02014 1 2e	7407.070(4)	1.17245(3)	0.35(3)		11/13	$2\nu_2+(\nu_4+4\nu_5)^3 - \nu_5^1$	$\Phi_g - \Pi_u$	6677.916(4)	R3-25	1.9	[19]
02014 1 2f	7407.073(3)	1.17232(2)	-0.10(2)		12/13	$2\nu_2+(\nu_4+4\nu_5)^3 - \nu_5^1$	$\Phi_g - \Pi_u$	6677.919(3)	R4-28	3.1	[19]
HW 20001 0 1e	7416.3997(4)	1.162904(2)	1.605(2)		74/74	$2\nu_1+\nu_5^1 - \nu_4^1$	$\Pi_u - \Pi_g$	6804.7059(4)	P35/Q17/R37	1.3	H [13,16]
HW 20001 0 1f	7416.4001(5)	1.167781(2)	1.661(2)		72/72	$2\nu_1+\nu_5^1 - \nu_4^1$	$\Pi_u - \Pi_g$	6804.7063(5)	P38/Q19/R38	1.1	H [13,16]
01103 0 3e	7421.901(8)	1.17087(4)	1.11(5)		8/12	$\nu_2+\nu_3+3\nu_5^3 - \nu_5^1$	$\Phi_g - \Pi_u$	6692.747(8)	R11-26	2.6	[19]
HW 11003 0 1f	7466.4503(7)	1.175696(6)	3.106(9)		43/49	$\nu_1+\nu_2+3\nu_5^1 - \nu_4^1$	$\Pi_u - \Pi_g$	6854.7565(7)	P28/Q1/R28	1.8	[18,19]
HW 11003 0 1e	7466.4552(6)	1.165633(6)	2.46(1)		50/52	$\nu_1+\nu_2+3\nu_5^1 - \nu_4^1$	$\Pi_u - \Pi_g$	6854.7614(6)	P27/Q8/R27	1.8	[18]
02005 0 1f	7509.783(1)	1.18194(1)	5.01(2)		18/20	$2\nu_2+5\nu_5^1 - \nu_4^1$	$\Pi_u - \Pi_g$	6898.089(1)	P24/R12	2.5	
02005 0 1e	7509.7941(9)	1.167650(9)	3.56(2)		21/24	$2\nu_2+5\nu_5^1 - \nu_4^1$	$\Pi_u - \Pi_g$	6898.1003(9)	P19/R23	2.4	[19]
***P*=12**											
02051 3-1f	7623.5680(8)	1.17233(1)	-1.81(3)		29/36	$2\nu_2+(5\nu_4+\nu_5)^2II - \nu_4^1$	$\Delta_u - \Pi_g$	7011.8742(8)	P19/Q21/R15	2.0	[19]
02051 3-1e	7623.576(2)	1.17201(5)	32.8(4)	424(8)	23/36	$2\nu_2+(5\nu_4+\nu_5)^2II - \nu_4^1$	$\Delta_u - \Pi_g$	7011.882(2)	P21/Q13/R17	2.1 **P**	[19]
02051 1-1e	7626.676(1)	1.17277(5)	-33.6(4)	-416(7)	21/29	$2\nu_2+(5\nu_4+\nu_5)^0 - \nu_4^1$	$\Sigma_u^+ - \Pi_g$	7014.982(1)	P13/Q20/R11	1.8	[19]
01140 2 0f	7661.588(1)	1.17045(2)	1.69(5)		26/26	$\nu_2+\nu_3+4\nu_4^2 - \nu_4^1$	$\Delta_u - \Pi_g$	7049.894(1)	P19/Q15/R6	1.1	[19]
HW 01140 2 0e	7661.591(1)	1.17047(3)	13.8(1)	92(1)	26/27	$\nu_2+\nu_3+4\nu_4^2 - \nu_4^1$	$\Delta_u - \Pi_g$	7049.897(1)	P24/Q15/R5	1.4	[19]
HW 01140 0 0e	7665.432(1)	1.17118(2)	-1.20(4)		17/20	$\nu_2+\nu_3+4\nu_4^0 - \nu_4^1$	$\Sigma_u^+ - \Pi_g$	7053.738(1)	P21/Q13/R2	4.6	
00220 2 0f	7685.4702(7)	1.169052(6)	2.333(9)		53/67	$2\nu_3+2\nu_4^2 - \nu_5^1$	$\Delta_g - \Pi_u$	6956.3161(7)	P31/Q30/R23	1.8	[18]
HW 00220 2 0e	7685.497(3)	1.1671(1)	34(2)	762(54)	18/45	$2\nu_3+2\nu_4^2 - \nu_5^1$	$\Delta_g - \Pi_u$	6956.343(3)	P26/ R24	2.3 **P**	[18,19]
00220 0 0e	7686.077(1)	1.1691(1)	-68(4)	-2984(260)	26/70	$2\nu_3+2\nu_4^0 - \nu_5^1$	$\Sigma_g^+ - \Pi_u$	6956.923(1)	P28/Q28/R22	0.5 **P**	[18]

	02042 4-2f	7702.0512(9)	1.17202(1)	3.78(2)		18/24	$2\nu_2+(4\nu_4+2\nu_5)^2$III - ν_5^1	$\Delta_g - \Pi_u$	6972.8971(9)	P21/Q26/R17	2.4	[19]
	02042 4-2e	7702.058(1)	1.17190(2)	14.7(1)	69(1)	19/20	$2\nu_2+(4\nu_4+2\nu_5)^2$III - ν_5^1	$\Delta_g - \Pi_u$	6972.904(1)	P25/Q9/R9	2.2	[19]
HW	02042 2-2e	7707.273(1)	1.17210(4)	-7.2(4)	-35(10)	30/33	$2\nu_2+(4\nu_4+2\nu_5)^0$II - ν_5^1	$\Sigma_g^+ - \Pi_u$	6978.119(1)	P17/Q16/R10	1.8	[19]
	11040 0 0e	7726.635(2)	1.17028(3)	-0.90(8)		14/15	$\nu_1+\nu_2+4\nu_4^0$ -ν_5^1	$\Sigma_g^+ - \Pi_u$	6997.481(2)	P20/R2	2.9	[19]
HW	10120 2 0f	7732.3512(8)	1.166835(6)	1.694(7)		80/83	$\nu_1+\nu_3+2\nu_4^2$ -ν_4^1	$\Delta_u - \Pi_g$	7120.6574(8)	P29/Q29/R25	0.3	+EDB17
	10120 2 0e	7732.368(2)	1.1652(1)	27(1)	574(34)	24/56	$\nu_1+\nu_3+2\nu_4^2$ -ν_4^1	$\Delta_u - \Pi_g$	7120.674(2)	P33/Q7/R26	4.2 **P**	+EDB17
	03021 2-1e	7734.43(2)	1.15874(4)	2.41(2)		7/8	$3\nu_2+(2\nu_4+\nu_5)^1$II - ν_4^1	$\Pi_u - \Pi_g$	7122.74(2)	P39-28	3.2	
	02042 2 0e	7734.713(2)	1.17253(7)	-15.4(5)		9/9	$2\nu_2+(4\nu_4+2\nu_5)^2$II - ν_5^1	$\Delta_g - \Pi_u$	7005.559(2)	P12/Q7/R9	3.1	
	01131 3-1f	7752.3318(8)	1.170860(7)	2.986(7)		16/17	$\nu_2+\nu_3+(3\nu_4+\nu_5)^2$II - ν_5^1	$\Delta_g - \Pi_u$	7023.1777(8)	P33/ R17	4.8	[19]
	01131 1 1f	7771.326(2)	1.1708(1)	16.2(9)		5/5	$\nu_2+\nu_3+(3\nu_4+\nu_5)^2$I- ν_5^1	$\Delta_g - \Pi_u$	7042.172(2)	P7/R9	5.1	
	01131 1 1e	7771.350(3)	1.16998(7)	11.8(4)		6/7	$\nu_2+\nu_3+(3\nu_4+\nu_5)^2$I- ν_5^1	$\Delta_g - \Pi_u$	7042.196(3)	P13/R8	4.5	[19]
	02042 0 2f	7777.888(2)	1.17183(2)	1.64(5)		8/10	$2\nu_2+(4\nu_4+2\nu_5)^2$I - ν_5^1	$\Delta_g - \Pi_u$	7048.734(2)	P18/Q20/R4	1.8	
	00211 1 1e	7810.15(1)	1.16889(2)	1.87(1)		7/10	$2\nu_3+(\nu_4+\nu_5)^2$ - $2\nu_4^2$	$\Delta_u - \Delta_g$	6581.35(1)	R24-38	2.1	
HW	02033 3-1f	7821.37(2)	1.17276(8)	4.27(9)		5/5	$2\nu_2+(3\nu_4+3\nu_5)^2$III -$2\nu_4^2$	$\Delta_u - \Delta_g$	6592.57(2)	R15-23	1.2	
HW	10111 1-1e	7834.9843(6)	1.168098(7)	4.11(2)	4.44(9)	55/63	$\nu_1+\nu_3+(\nu_4+\nu_5)^{0+}$- ν_5^1	$\Sigma_g^+ - \Pi_u$	7105.8303(5)	P38/Q23/R22	1.0	+EDB17, [19]
HW	10111 1 1f	7847.7499(7)	1.167403(8)	1.66(2)	-0.6(2)	64/68	$\nu_1+\nu_3+(\nu_4+\nu_5)^2$- ν_5^1	$\Delta_g - \Pi_u$	7118.5956(7)	P35/Q27/R20	1.4	+EDB17
HW	10111 1 1e	7847.751(1)	1.16737(2)	-0.7(1)	-6(2)	41/52	$\nu_1+\nu_3+(\nu_4+\nu_5)^2$- ν_5^1	$\Delta_g - \Pi_u$	7118.5969(9)	P32/Q21/R20	1.6	+EDB17
HW	10111 1-1f	7853.2767(6)	1.167492(5)	1.657(6)		39/43	$\nu_1+\nu_3+(\nu_4+\nu_5)^0$- ν_5^1	$\Sigma_g^+ - \Pi_u$	7124.1222(6)	P30/Q18/R19	1.6	+EDB17
HW	01122 2-2e	7858.588(3)	1.17224(3)	9.36(6)		7/8	$\nu_2+\nu_3+(2\nu_4+2\nu_5)^0$II - $2\nu_4^0$	$\Sigma_u^+ - \Sigma_g^+$	6628.199(3)	R4-19	2.3	
	00202 0 0e	7922.27(2)	1.16908(7)	3.39(5)		8/8	$2\nu_3+2\nu_5^0$- $(\nu_4+\nu_5)^{0+}$	$\Sigma_g^+ - \Sigma_u^+$	6594.20(2)	R19-27	1.8	
HW	02024 2-2e	7930.409(5)	1.17191(3)	6.30(4)		8/15	$2\nu_2+(2\nu_4+4\nu_5)^0$II -$(\nu_4+\nu_5)^{0+}$	$\Sigma_g^+ - \Sigma_u^+$	6651.859(3)	R11-32	1.6 **P**	
	00202 0 2e	7930.78(2)	1.17039(5)	0.83(3)		5/5	$2\nu_3+2\nu_5^2$- $(\nu_4+\nu_5)^2$	$\Delta_g - \Delta_u$	6587.98(2)	R22-32	2.6	
	00202 0 2f	7930.807(7)	1.16987(2)	1.71(1)		9/10	$2\nu_3+2\nu_5^2$- $(\nu_4+\nu_5)^2$	$\Delta_g - \Delta_u$	6588.005(1)	R18-33	2.1	
	02024-2 4e	7939.94(2)	1.1755(1)	3.1(1)		4/5	$2\nu_2+(2\nu_4+4\nu_5)^2$III - $(\nu_4+\nu_5)^2$	$\Delta_g - \Delta_u$	6597.14(2)	R14-22	3.6	
	02024-2 4f	7940.303(5)	1.17251(2)	2.19(2)		10/12	$2\nu_2+(2\nu_4+4\nu_5)^2$III - $(\nu_4+\nu_5)^2$	$\Delta_g - \Delta_u$	6597.501(5)	R13-26	2.0	
	10102 0 0e	7961.818(1)	1.16853(3)	5.0(2)		14/17	$\nu_1+\nu_3+2\nu_5^0$ - $2\nu_4^0$	$\Sigma_u^+ - \Sigma_g^+$	6731.429(1)	P14/R15	1.9	[19]
	10102 0 2f	7971.557(1)	1.16806(2)	1.85(3)		14/17	$\nu_1+\nu_3+2\nu_5^2$ - $2\nu_4^2$	$\Delta_u - \Delta_g$	6742.757(1)	P21/R20	1.7	[19]
	10102 0 2e	7971.5609(9)	1.168100(6)			5/8	$\nu_1+\nu_3+2\nu_5^2$ - $2\nu_4^0$	$\Delta_u - \Sigma_g^+$	6741.1715(9)	P20-7	2.4	[19]
						8/15	$\nu_1+\nu_3+2\nu_5^2$ - $2\nu_4^2$	$\Delta_u - \Delta_g$	6742.7598(9)	P9/Q6/R15	2.0	[19]
HW	20011 1-1e	7994.3951(7)	1.16731(2)	3.87(6)		29/54	$2\nu_1+(\nu_4+\nu_5)^{0+}$ - $2\nu_4^0$	$\Sigma_u^+ - \Sigma_g^+$	6764.0057(7)	P28/R29	1.3 **P**	[18]
						15/43	$2\nu_1+(\nu_4+\nu_5)^{0+}$ - $2\nu_4^2$	$\Sigma_u^+ - \Delta_g$	6765.5940(7)	P31/R35	1.7 **P**	[19]
	02024 0 2e	7994.662(2)	1.173542(5)			7/9	$2\nu_2+(2\nu_4+4\nu_5)^2$I -$(\nu_4+\nu_5)^2$	$\Delta_g - \Delta_u$	6651.859(3)	R3-20	3.0	[19]
	01113-1 3f	8003.610(1)	1.17244(2)	0.55(6)		12/12	$\nu_2+\nu_3+(\nu_4+3\nu_5)^2$I - $(\nu_4+\nu_5)^2$	$\Delta_g - \Delta_u$	6660.808(1)	P7/Q2/R17	1.8	[19]
	01113-1 3e	8003.611(1)	1.17240(2)	0.76(5)		10/11	$\nu_2+\nu_3+(\nu_4+3\nu_5)^2$I - $(\nu_4+\nu_5)^2$	$\Delta_g - \Delta_u$	6660.808(1)	P11/Q5/R18	1.5	[19]
HW	20011 1 1e	8008.2358(9)	1.16662(2)	-0.20(6)		13/41	$2\nu_1+(\nu_4+\nu_5)^2$ - $2\nu_4^0$	$\Delta_u - \Sigma_g^+$	6777.8464(9)	P30/R33	1.4 **P**	[19]

HW					33/43	$2\nu_1+(\nu_4+\nu_5)^2 - 2\nu_4^2$	$\Delta_u - \Delta_g$	6779.4347(9)	P21/Q16/R21	1.0 **P**	[18]
HW 20011 1 1f	8008.2360(6)	1.166626(4)	1.647(5)		54/54	$2\nu_1+(\nu_4+\nu_5)^2 - 2\nu_4^2$	$\Delta_u - \Delta_g$	6779.4363(6)	P30/Q15/R28	1.1	[18]
11013 1-1e	8025.670(2)	1.17300(3)	9.5(1)		10/11	$\nu_1+\nu_2+(\nu_4+3\nu_5)^{0+} - 2\nu_4^0$	$\Sigma_u^+ - \Sigma_g^+$	6795.281(2)	P16/R11	1.4	[19]
HW 01104 0 0e	8101.870(2)	1.17325(3)	9.14(6)		9/12	$\nu_2+\nu_3+4\nu_5^0 - 2\nu_5^0$	$\Sigma_u^+ - \Sigma_g^+$	6652.759(2)	P4/R18	2.3	[19]
01104 0 2f	8113.527(2)	1.17356(2)	-0.55(2)		7/9	$\nu_2+\nu_3+4\nu_5^2 - 2\nu_5^2$	$\Delta_u - \Delta_g$	6655.233 (2)	P8/R24	2.5	[19]
HW 20002 0 0e	8114.3615(7)	1.167966(8)	4.62(2)	7.3(2)	51/51	$2\nu_1+2\nu_5^0 - (\nu_4+\nu_5)^{0+}$	$\Sigma_g^+ - \Sigma_u^+$	6786.2893(7)	P28/R30	1.3	[18,19]
20002 0 2f	8123.7609(7)	1.167412(5)	1.667(5)		46/48	$2\nu_1+2\nu_5^2 - (\nu_4+\nu_5)^2$	$\Delta_g - \Delta_u$	6780.9586(7)	P29/Q14/R29	1.8	[18]
20002 0 2e	8123.7631(8)	1.167353(9)	-1.25(2)	-7.2(2)	47/47	$2\nu_1+2\nu_5^2 - (\nu_4+\nu_5)^2$	$\Delta_g - \Delta_u$	6780.9597(8)	P28/Q15/R30	1.8	[18]
HW 11004 0 0e	8164.558(2)	1.17317(4)	9.5(2)		14/14	$\nu_1+\nu_2+4\nu_5^0 - (\nu_4+\nu_5)^{0+}$	$\Sigma_g^+ - \Sigma_u^+$	6836.486(2)	P10/R13	0.6	[19]
11004 0 2e	8173.766(1)	1.17274(3)	-5.0(1)		14/14	$\nu_1+\nu_2+4\nu_5^2 - (\nu_4+\nu_5)^2$	$\Delta_g - \Delta_u$	6830.963(1)	P16/Q3/R14	1.6	[19]
11004 0 2f	8173.769(1)	1.17270(2)	2.64(4)		19/19	$\nu_1+\nu_2+4\nu_5^2 - (\nu_4+\nu_5)^2$	$\Delta_g - \Delta_u$	6830.967(1)	P19/Q2/R19	1.9	[19]
***P*=13**											
00230 3 0e	8285.037(3)	1.17136(8)	42.3(8)	621(19)	11/11	$2\nu_3+3\nu_4^3 - (\nu_4+\nu_5)^2$	$\Phi_g - \Delta_u$	6942.234(3)	P16/Q7/R10	2.2	[19]
					7/7	$2\nu_3+3\nu_4^3 - (\nu_4+\nu_5)^0$	$\Phi_g - \Sigma_u^+$	6956.965(3)	P8-16	2.4	[19]
00230 3 0f	8285.072(3)	1.16932(6)	6.3(3)		12/13	$2\nu_3+3\nu_4^3 - (\nu_4+\nu_5)^2$	$\Phi_g - \Delta_u$	6942.270(3)	P13/Q7/R13	1.5	[19]
00230 1 0f	8286.4139(9)	1.17719(3)	-7.5(3)	-135(6)	22/27	$2\nu_3+3\nu_4^1 - (\nu_4+\nu_5)^2$	$\Pi_g - \Delta_u$	6943.6116(9)	P18/Q17	2.0	[19]
					16/21	$2\nu_3+3\nu_4^1 - (\nu_4+\nu_5)^0$	$\Pi_g - \Sigma_u$	6945.8632(9)	P13/Q14/R9	2.4	[19]
00230 1 0e	8286.422(1)	1.16405(4)	-33.6(5)	-487(13)	12/14	$2\nu_3+3\nu_4^1 - (\nu_4+\nu_5)^2$	$\Pi_g - \Delta_u$	6943.619(1)	P10/Q15	2.5	[19]
					18/25	$2\nu_3+3\nu_4^1 - (\nu_4+\nu_5)^0$	$\Pi_g - \Sigma_u$	6958.350(1)	P16/Q13/R14	2.2	[19]
03031 1-1e	8319.92(2)	1.17143(9)	11.3(1)		6/6	$3\nu_2+(3\nu_4+\nu_5)^0 - 2\nu_4^0$	$\Sigma_u^+ - \Sigma_g^+$	7089.53(2)	P22-15	1.7	
10130 3 0e	8329.303(3)	1.1677(2)	31(1)		9/20	$\nu_1+\nu_3+3\nu_4^3 - 2\nu_4^2$	$\Phi_u - \Delta_g$	7100.502(3)	P25/R11	2.4 **P**	+EDB17
10130 3 0f	8329.39(1)	1.16592(5)	1.89(5)		8/9	$\nu_1+\nu_3+3\nu_4^3 - 2\nu_4^2$	$\Phi_u - \Delta_g$	7100.59(1)	P28-16	1.9	
01141 2 1e	8382.619(3)	1.16881(4)	-3.6(1)		6/6	$\nu_2+\nu_3+(4\nu_4+\nu_5)^3I - (\nu_4+\nu_5)^2$	$\Phi_g - \Delta_u$	7039.816(3)	P18-5	2.0	
HW 00221 0 1e	8398.716(1)	1.16981(1)	1.0(2)		11/14	$2\nu_3+(2\nu_4+\nu_5)^1I - 2\nu_5^0$	$\Pi_u - \Sigma_g^+$	6949.605(1)	P25/R17	2.6	
					8/8	$2\nu_3+(2\nu_4+\nu_5)^1I - 2\nu_5^2$	$\Pi_u - \Delta_g$	6940.422(1)	P19-3	2.5	
HW 10121 2-1f	8419.500(1)	1.174864(8)	3.34(1)		18/20	$\nu_1+\nu_3+(2\nu_4+\nu_5)^1II-(\nu_4+\nu_5)^2$	$\Pi_g - \Delta_u$	7076.698(1)	P28-5	2.4	
					6/6	$\nu_1+\nu_3+(2\nu_4+\nu_5)^1II-(\nu_4+\nu_5)^0$	$\Pi_g - \Sigma_u^-$	7078.949(1)	P23-7	2.5	
HW 10121 2-1e	8419.504(1)	1.164901(6)	2.722(6)		10/12	$\nu_1+\nu_3+(2\nu_4+\nu_5)^1II-(\nu_4+\nu_5)^2$	$\Pi_g - \Delta_u$	7076.701(1)	P26-6	2.4	
					9/10	$\nu_1+\nu_3+(2\nu_4+\nu_5)\,^1II-(\nu_4+\nu_5)^0$	$\Pi_g - \Sigma_u^+$	7091.432(1)	P34-13	2.0	
12020 2 0e	8432.807(6)	1.16166(3)	-1.40(5)		5/5	$\nu_1+2\nu_2+2\nu_4^2 - (\nu_4+\nu_5)^2$	$\Delta_g - \Delta_u$	7090.004(6)	P24-12	0.6	
12020 2 0f	8432.900(6)	1.160699(5)	2.12(7)		4/4	$\nu_1+2\nu_2+2\nu_4^2 - (\nu_4+\nu_5)^2$	$\Delta_g - \Delta_u$	7090.098(6)	P23-12	1.2	
10112 1 0f	8531.565(1)	1.175749(7)	3.008(7)		12/12	$\nu_1+\nu_3+(\nu_4+2\nu_5)^1II - 2\nu_5^2$	$\Pi_u - \Delta_g$	7073.271(1)	P32-5	4.0	
10112 1 0e	8531.5788(9)	1.165171(6)	2.333(7)		15/17	$\nu_1+\nu_3+(\nu_4+2\nu_5)^1II - 2\nu_5^0$	$\Pi_u - \Sigma_g^+$	7082.4681(9)	P31-7	2.5	
					13/13	$\nu_1+\nu_3+(\nu_4+2\nu_5)^1II - 2\nu_5^2$	$\Pi_u - \Delta_g$	7073.2844(9)	P25/Q26	3.9	
10112 1 2e	8554.981(3)	1.16960(1)	1.24(1)		6/9	$\nu_1+\nu_3+(\nu_4+2\nu_5)^3 - 2\nu_5^2$	$\Phi_u - \Delta_g$	7096.687(3)	P32-13	2.4	

10112 1 2f	8555.111(4)	1.16896(2)	0.33(1)		7/8	$\nu_1+\nu_3+(\nu_4+2\nu_5)^3 - 2\nu_5^2$	$\Phi_u - \Delta_g$	7096.817(4)	P32-13	1.6	
10112-1 2f	8556.902(6)	1.16734(4)	1.69(5)		6/7	$\nu_1+\nu_3+(\nu_4+2\nu_5)^1I - 2\nu_5^2$	$\Pi_u - \Delta_g$	7098.608(6)	P25-13	1.7	
10112-1 2e	8556.903(6)	1.17202(3)	1.85(2)		7/9	$\nu_1+\nu_3+(\nu_4+2\nu_5)^1I - 2\nu_5^2$	$\Pi_u - \Delta_g$	7098.609(6)	P29-16	1.3	
HW 20021 2-1e	8580.299(2)	1.16549(3)	3.4(1)		15/19	$2\nu_1+(2\nu_4+\nu_5)^1II - 3\nu_4^1$	$\Pi_u - \Pi_g$	6725.701(2)	P14/R16	1.4	[19]
HW 20021 2-1f	8580.309(2)	1.17198(2)	1.45(9)	-29.9(9)	16/20	$2\nu_1+(2\nu_4+\nu_5)^1II - 3\nu_4^1$	$\Pi_u - \Pi_g$	6725.712(2)	P16/R24	1.9	[19]
03013 1-1e	8582.43(1)	1.16010(6)	-1.66(9)		6/6	$3\nu_2+(\nu_4+3\nu_5)^0 - 3\nu_4^1$	$\Sigma_u^+ - \Pi_g$	6727.83(1)	P23/R18	3.0	
10103 0 3e	8679.460(1)	1.169584(6)			6/9	$\nu_1+\nu_3+3\nu_5^3 - (2\nu_4+\nu_5)^3$	$\Phi_g - \Phi_u$	6717.527(1)	P7/R18	1.2	[19]
20012-1 2f	8695.0397(7)	1.174227(7)	3.16(1)		20/23	$2\nu_1+(\nu_4+2\nu_5)^1II - (2\nu_4+\nu_5)^1I$	$\Pi_g - \Pi_u$	6735.3476(7)	P18/R23	2.8	[19]
					20/23	$2\nu_1+(\nu_4+2\nu_5)^1II - (2\nu_4+\nu_5)^1II$	$\Pi_g - \Pi_u$	6755.0410(7)	P23/R20	1.5	[19]
20012-1 2e	8695.0444(7)	1.165037(8)	2.52(1)		12/16	$2\nu_1+(\nu_4+2\nu_5)^1II - (2\nu_4+\nu_5)^1I$	$\Pi_g - \Pi_u$	6735.3528(7)	P12/R18	3.7	[19]
					26/28	$2\nu_1+(\nu_4+2\nu_5)^1II - (2\nu_4+\nu_5)^1II$	$\Pi_g - \Pi_u$	6755.0445(7)	P24/R22	1.8	[19]
20012 1 2e	8720.297(1)	1.16841(2)	0.93(5)		17/19	$2\nu_1+(\nu_4+2\nu_5)^3 - (2\nu_4+\nu_5)^3$	$\Phi_g - \Phi_u$	6758.364(1)	P20/Q7/R20	1.3	[19]
20012 1 2f	8720.298(1)	1.16837(2)	0.75(4)		17/17	$2\nu_1+(\nu_4+2\nu_5)^3 - (2\nu_4+\nu_5)^3$	$\Phi_g - \Phi_u$	6758.366(1)	P21/Q6/R19	1.8	[19]
20003 0 1f	8812.423(3)	1.17536(4)	3.0(1)		9/9	$2\nu_1+3\nu_5^1 - (\nu_4+2\nu_5)^1II$	$\Pi_u - \Pi_g$	6764.547(3)	P16/R16	0.9	[19]
20003 0 1e	8812.433(2)	1.16514(4)	2.1(1)		8/9	$2\nu_1+3\nu_5^1 - (\nu_4+2\nu_5)^1II$	$\Pi_u - \Pi_g$	6764.557(2)	P15/R15	1.6	[19]
HW 20003 0 3e	8831.146(2)	1.16927(2)	0.76(7)		12/12	$2\nu_1+3\nu_5^3 - (\nu_4+2\nu_5)^3$	$\Phi_u - \Phi_g$	6756.967(2)	P15/Q4/R17	1.4	[19]
HW 20003 0 3f	8831.147(2)	1.16924(3)	0.54(9)		12/12	$2\nu_1+3\nu_5^3 - (\nu_4+2\nu_5)^3$	$\Phi_u - \Phi_g$	6756.966(2)	P16/Q5/R16	1.6	[19]
***P*=14**											
10131 3 1f	9034.784(5)	1.17057(3)	2.77(4)		4/5	$\nu_1+\nu_3+(3\nu_4+\nu_5)^4 - (2\nu_4+\nu_5)^1I$	$\Gamma_g - \Pi_u$	7075.092(5)	P25-15	4.1	
					5/6	$\nu_1+\nu_3+(3\nu_4+\nu_5)^4 - (2\nu_4+\nu_5)^3$	$\Gamma_g - \Phi_u$	7072.852(5)	P25-13	6.5	
10131 3 1e	9034.908(3)	1.16967(2)	1.28(3)		5/6	$\nu_1+\nu_3+(3\nu_4+\nu_5)^4 - (2\nu_4+\nu_5)^3$	$\Gamma_g - \Phi_u$	7072.975(3)	P25-6	2.3	
10131 1 1e	9041.200(3)	1.17116(2)	1.25(3)		6/6	$\nu_1+\nu_3+(3\nu_4+\nu_5)^2I - (2\nu_4+\nu_5)^1I$	$\Delta_g - \Pi_u$	7081.508(3)	P26-8	1.8	
10122 0 0e	9104.211(2)	1.17230(2)	7.99(6)		8/8	$\nu_1+\nu_3+(2\nu_4+2\nu_5)^0II-(\nu_4+2\nu_5)^1II$	$\Sigma_u^+ - \Pi_g$	7056.335(2)	P20-4	6.0	
10113 1 1e	9229.634(3)	1.17288(3)	-3.60(6)		9/13	$\nu_1+\nu_3+(\nu_4+3\nu_5)^2II - 3\nu_5^1$	$\Delta_g - \Pi_u$	7060.476(3)	P14/Q20	4.0	
10113 1 1f	9229.651(1)	1.17256(1)	2.52(1)		14/17	$\nu_1+\nu_3+(\nu_4+3\nu_5)^2II - 3\nu_5^1$	$\Delta_g - \Pi_u$	7060.495(1)	P20/Q26	3.5	
$^{12}C^{13}CH_2$											
00000 0 0	0.0	1.1484335	1.5256								
00010 1 0e	608.3535	1.147100	1.592								
00010 1 0f	608.3535	1.152127	1.640								
00001 0 1f	728.2282	1.152682	1.586								
00001 0 1e	728.2293	1.148195	1.544								
HW 01102 0 0e	6650.2672(5)	1.141140(7)	3.94(2)	5.4(1)	34/34	$\nu_2+\nu_3+2\nu_5^0$	$\Sigma^- - \Sigma$	6650.2672(5)	P9/R31	1.2	
HW 20000 0 0e	6686.5292(5)	1.135719(6)	1.56(1)		33/33	$2\nu_1$	$\Sigma^- - \Sigma$	6686.5292(5)	P20/R23	1.3	

HW 11002 0 0e	6713.7069(6)	1.14095(1)	4.68(3)	7.5(3)	35/36	$\nu_1+\nu_2+2\nu_5^0$	$\Sigma^-\Sigma$	6713.7069(6)	P19/R27	1.4	
02004 0 0e	6737.0599(7)	1.14370(2)	7.61(7)		20/21	$2\nu_2+4\nu_5^0$	$\Sigma^-\Sigma$	6737.0599(7)	P17/R13	1.9	
HW 01130 1 0f	6999.629(1)	1.14586(3)	-1.34(9)		10/10	$\nu_2+\nu_3+3\nu_4^1$	$\Pi^-\Sigma$	6999.629(1)	Q16	2.0	
HW 01130 1 0e	6999.6375(8)	1.13509(2)	-6.9(1)	-20(2)	26/30	$\nu_2+\nu_3+3\nu_4^1$	$\Pi^-\Sigma$	6999.6375(8)	P22/R17	2.2	
03011 1-1e	7063.485(1)	1.13353(1)	3.01(2)		13/16	$3\nu_2+(\nu_4+\nu_5)^{0+}$	$\Sigma^-\Sigma$	7063.485(1)	P24/R17	2.6	+EDB17
HW 00210 1 0e	7078.9357(8)	1.135791(4)	1.475(4)		19/22	$2\nu_3+\nu_4^1$	$\Pi^-\Sigma$	7078.9357(8)	P35/R7	1.7	+FTS15
HW 00210 1 0f	7078.936(1)	1.14153(2)	1.53(5)		12/13	$2\nu_3+\nu_4^1$	$\Pi^-\Sigma$	7078.936(1)	Q18	1.9	+FTS15
00201 0 1e	7205.01(1)	1.13767(5)	1.91(4)		6/8	$2\nu_3+\nu_5^1-\nu_4^1$	$\Pi-\Pi$	6596.66(1)	R18-27	2.4	
00201 0 1f	7205.020(4)	1.14243(2)	1.94(1)		8/10	$2\nu_3+\nu_5^1-\nu_4^1$	$\Pi-\Pi$	6596.670(4)	R14-29	2.1	
01112 1 0f	7230.190(5)	1.14662(8)	2.8(2)		3/3	$\nu_2+\nu_3+(\nu_4+2\nu_5)^1\mathrm{II}-\nu_4^1$	$\Pi-\Pi$	6621.837(5)	R6-16	0.0	
01112 1 0e	7230.207(2)	1.13740(3)	2.29(9)		6/8	$\nu_2+\nu_3+(\nu_4+2\nu_5)^1\mathrm{II}-\nu_4^1$	$\Pi-\Pi$	6621.854(2)	R5-17	2.0	
HW 20010 1 0f	7272.4527(6)	1.139557(4)	1.607(5)		29/30	$2\nu_1+\nu_4^1-\nu_4^1$	$\Pi-\Pi$	6664.0992(6)	P13/R29	1.3	
HW 20010 1 0e	7272.4540(7)	1.134675(5)	1.564(7)		23/24	$2\nu_1+\nu_4^1-\nu_4^1$	$\Pi-\Pi$	6664.1005(7)	P14/R27	1.0	
20001 0 1f[h]	7393.0206(9)	1.140330(7)	1.66(1)		18/19	$2\nu_1+\nu_5^1-\nu_5^{1\,h}$	$\Pi-\Pi$	6664.7924(9)	P12/R25	1.7	
20001 0 1e[h]	7393.022(1)	1.135476(7)	1.534(8)		13/14	$2\nu_1+\nu_5^1-\nu_5^{1\,h}$	$\Pi-\Pi$	6664.793(1)	P12/R28	1.4	
HW 20001 0 1e[h]	7394.1688(5)	1.135527(3)	1.582(4)		41/43	$2\nu_1+\nu_5^1-\nu_4^{1\,h}$	$\Pi-\Pi$	6785.8153(5)	P28/R29	0.9	
HW 20001 0 1f[h]	7394.1695(5)	1.140367(3)	1.696(4)		39/40	$2\nu_1+\nu_5^1-\nu_4^{1\,h}$	$\Pi-\Pi$	6785.8160(5)	P28/R29	0.9	
11003 0 1f	7420.656(1)	1.14827(2)	3.13(5)		16/16	$\nu_1+\nu_2+3\nu_5^1-\nu_4^1$	$\Pi-\Pi$	6812.303(1)	P13/R17	2.0	
11003 0 1e	7420.658(1)	1.13807(2)	2.55(4)		17/21	$\nu_1+\nu_2+3\nu_5^1-\nu_4^1$	$\Pi-\Pi$	6812.305(1)	P19/R17	1.7	
00220 0 0e	7675.572(7)	1.14310(6)	-2.8(1)		10/11	$2\nu_3+2\nu_4^0-\nu_4^1$	$\Sigma^-\Pi$	7067.219(7)	P18/Q18	2.2	
02110 1 0e	7719.285(8)	1.12949(3)	1.57(3)		6/8	$2\nu_2+\nu_3+\nu_4^1-\nu_4^1$	$\Pi-\Pi$	7110.932(8)	P29-18	1.6	
02110 1 0f	7719.298(6)	1.13463(2)	1.58(2)		10/13	$2\nu_2+\nu_3+\nu_4^1-\nu_4^1$	$\Pi-\Pi$	7110.945(6)	P30-18	1.6	
$^{12}C_2HD$											
00000 0 0	0.0	0.991538	1.141								
HW 01200 0 0e	6932.191(1)	0.97411(1)	1.18(2)	0.8(1)	49/52	$\nu_2+2\nu_3$	$\Sigma^-\Sigma$	6932.193(1)	P34/R35	1.2	
12000 0 0e	7018.105(2)	0.97818(1)	-0.50(2)		16/28	$\nu_1+2\nu_2$	$\Sigma^-\Sigma$	7018.105(2)	P20/R28	5.6	
10111 1 1e	7073.902(3)	0.98397(1)	-3.78(1)		13/24	$\nu_1+\nu_2+(\nu_4+\nu_5)^{0+}$	$\Sigma^-\Sigma$	7073.902(3)	P35-4	5.8	

Notes.

The confidence interval (1 SD) is given in parenthesis in the unit of the last quoted digit.

[a] Normal mode labeling: $v_{i=1-5}$ are the vibrational quantum numbers, $l_{4,5}$ are the vibrational angular momentum quantum numbers associated to the degenerate bending modes and $\varepsilon=e$ or f is the symmetry type relative to the Wang transformation. The labeling was obtained according to the maximum value of the modulo of the expansion coefficients of the vibrational eigenfunction in the normal mode basis (for low J values) (except for the bands with upper levels at 7051.01, 7054.34, 7228.27, 7734.71 and at 9104.21 cm^{-1}, see text for details).

[b] N_{tot} is the total number of observed transitions reaching a given vibrational state and n_{fit} is the number of positions included in the fit of the parameters. Only total number of observed lines is given in the cases where no fit has been performed.
[c] Observed band in Plíva notation.
[d] Band center. $\Delta G_c = G_c^{'} - G_c^{''}$
[e] Observed branches with maximum value or range of the total angular momentum quantum number.
[f] Root mean square deviation in 10^{-3} cm^{-1} unit. "P" marks perturbed states.
[g] +H, +EDB17, +FTS15 means that the present CRDS set of line positions was completed with values from HITRAN2016, our empirical database [2] and Ref. [3], respectively, in order to fit the spectroscopic parameters. Previous observations of the considered band are indicated for the principal isotopologue, when available. An asterisk '*'indicates that the band labeling was modified compared to previous works.
[h] Following Ref. [28], we give the same vibrational labeling -2000101- to the $^{12}C^{13}CH_2$ energy levels at 7393.02 and 7394.17 cm^{-1} although the upper level of the two bands are distinct (see Text).

Table 3.
The obtained values of dipole moment squared and Herman-Wallis factors. The calculated line position and intensities were presented in the recommended line list for these bands.

	Band[a]	ΔG_c[b]	N_{exp}[c]	*rms (%)* [d]	N_{tot}[e]	Transitions[f]	$\|R_0\|^2 in$ D^2	$A_1^{RP} \times 10^2$	$A_2^{RP} \times 10^3$	$A_2^{Q} \times 10^3$	Note[g]
261	1010000- 0000000	6556.465	62	1.9	77	P22/R54	1.150(4)E-04	-0.05(1)	0.023(4)		HITRAN
261	020333-1f-0002020	6592.570	4	4.4	23	R24	2.54(6)E-06				
261	110212-1- 0001010	6594.257	118	2.1	126	P31/R35	3.84(1)E-6	-0.141(5)	0.01(3)		HITRAN
261	1101210- 0000101	6600.187	120	3.3	134	P31/R39	2.003(9)E-06		-0.063(4)		HITRAN
261	0020101f- 0001010	6606.506	52	1.8	62	P20/R41	1.920(5)E-06				HITRAN
261	0020101e- 0001010	6606.507	63	1.5	73	P31/R43	1.923(5)E-06		0.106(3)		HITRAN
261	1102121f- 0001010	6616.371	27	5.2	39	R41	9.6(6)E-10	2.9(4)	-0.63(9)		
261	020232-1e- 0001010	6616.566	36	4.8	41	P17/R25	1.57(2)E-6	0.14(2)	-1.40(2)		HITRAN
261	020232-1f- 0001010	6616.584	47	3.7	52	P25/R28	1.56(1)E-6		-0.633(3)		HITRAN
261	11012-12- 0000101	6620.987	30	7.2	60	R32	1.00(1)E-07				
261	1102101f- 0001010	6622.598	19	10.2	30	R30	1.4(2)E-08	8.1(8)			
261	110111-1- 0000000	6623.136	61	1.8	69	P24/R44	1.482(5)E-06	-0.057(9)	-0.073(3)		HITRAN
261	011222-2e-0002000	6628.199	6	10.3	15	R14	3.8(2)E-07				
261	02014-12-0000101	6633.588	17	9.9	40	R25	4.5(3)E-08				
262	0110200- 0000000	6650.267	23	5.2	39	P10/R28	6.0(7)E-07				
261	020242-2e-000111-1	6651.859	8	11.1	23	R22	1.86(8)E-06				
261	0110400- 0000200	6652.759	11	10.0	25	P5/R19	2.17(7)E-07				
261	020131-1-0000000	6654.252	50	4.0	56	P21/R34	2.28(2)E-08		-0.336(7)		HITRAN
261	0111210- 0001010	6662.076	47	5.6	70	P11/R25	2.94(4)E-08	-0.23(4)			
262	2001010- 0001010	6664.100	34	6.8	78	P15/R26	2.59(3)E-06				
261	0202301f- 0001010	6666.780	19	10.4	40	P11/R30	2.6(2)E-09		1.9(2)		
261	0202301e- 0001010	6666.784	12	7.9	30	P8/R23	3.2(1)E-09	-1.2(1)			
261	0110301- 0000101	6672.229	56	6.3	91	P15/Q13/R27	1.10(1)E-07	-0.16(4)			
261	01112-12f-0001010	6674.430	18	5.5	39	P19/Q2/R19	3.6(1)E-08	-0.27(5)	-0.27(7)		
262	2000000- 0000000	6686.529	29	2.6	46	P21/R24	1.702(8)E-06				
261	0110200- 0000000	6690.576	57	3.0	66	P31/R34	5.58(3)E-08	-0.19(1)	-0.251(6)		HITRAN
262	1100200- 0000000	6713.707	27	5.4	49	P20/R28	8.5(1)E-08		-0.10(2)		
261	200212-1- 0003010	6725.706	26	8.5	65	P15/R22	4.48(8)E-07				
261	2000303- 0001212	6756.967	18	5.7	65	P17/Q6/R18	7.2(1)E-07				
261	200111-1-0002000	6764.006	42	6.8	55	P28/R29	3.34(5)E-07		-0.56(2)		Exp. **P**

261	2001111- 0002000	6777.846	29	8.0	56	P30/R33	7.5(1)E-10	-0.54(4)			Exp. **P**
261	2001111e- 0002020	6779.435	36	6.2	52	P21/Q16/R21	2.95(4)E-07		-0.59(3)		Exp. **P**
261	2001111f- 0002020	6779.436	36	3.7	54	P21/Q10/R27	2.99(2)E-07				
262	2000101- 0001010	6785.815	67	4.8	110	P29/R30	1.12(1)E-06		0.08(1)		
261	2000200- 000111-1	6786.289	41	5.9	61	P29/R31	2.84(3)E-07				
261	2000101- 0001010	6804.706	108	4.1	167	P31/Q20/R37	1.602(7)E-07	-0.03(1)		-1.19(3)	
261	1100400- 000111-1	6836.486	10	6.6	26	P11/R14	1.44(3)E-08				
261	1100301- 0001010	6854.759	75	4.4	119	P29/Q8/R29	4.15(2)E-09	-0.09(2)			
263	0120000- 0000000	6932.193	35	9.2	62	P31/R30	2.43(4)E-06				
261	0022101- 0000200	6949.605	11	7.8	34	P26/R8	1.57(8)E-08		1.2(1)		
261	0022020e- 0000101	6956.343	30	9.5	48	P26/R24	1.17(4)E-08	-1.32(7)	0.47(6)		Exp. **P**
261	020422-2e-0000101	6978.119	18	9.2	41	P17/Q14/R10	2.19(5)E-09				
262	0113010- 0000000	6999.637	21	10.3	44	P16/Q17/R11	2.98(7)E-08				
261	020412-1- 0000000	7015.952	38	10.0	62	P26/Q24/R12	1.18(2)E-09				
261	0114020e-0001010	7049.897	21	10.7	42	P24/Q16/R5	1.68(8)E-08	-3.1(2)		-1.8(2)	
261	0114000-0001010	7053.738	11	7.5	23	P12/Q11	2.46(8)E-08	-0.9(3)			
261	101212-1f-0001111	7076.698	11	6.8	28	P29	1.8(1)E-07	-4.0(4)			
261	101212-1e-0001111	7076.701	8	8.5	26	P27	2.85(9)E-07				
262	0021010- 0000000	7078.937	24	10.2	57	P30/Q19/R8	6.1(2)E-7	-0.7(1)			
261	101111-1e-0000101	7105.830	45	4.7	80	P37/Q24/R19	4.71(6)E-07	-1.08(4)	0.56(3)	-0.17(4)	EDB17
261	1011111f- 0000101	7118.596	47	6.2	78	P35/Q25/R21	5.64(7)E-07	-1.06(4)	0.07(2)		EDB17
261	1011111e- 0000101	7118.597	35	6.2	64	P24/Q22/R21	5.6(1)E-07	-0.81(4)	-0.36(3)	0.26(6)	EDB17
261	1012020f-0001010	7120.657	77	1.3	83	P30/Q30/R26	7.57(1)E-07	-0.967(6)			EDB17
261	101111-1f-0000101	7124.122	30	7.6	62	P31/Q19/R12	1.74(3)E-07	-1.59(8)		0.4(1)	EDB17
261	1011010- 0000000	7141.503	97	1.9	110	P44/Q34/R32	8.40(2)E-07	-1.037(6)			HITRAN

Notes

[a] Band vibrational labeling, ($V_1V_2V_3V_4V_5l_4l_5$)

[b] Band center in cm^{-1}

[c] $N_{exp}$is the number of measured line intensities included in the fit of the Herman-Wallis coefficients (see SupMat 2).

[d] Root mean square deviation of the intensity fit in %.

[e] N_{tot} is the total number of lines included in our recommended list (see SupMat 3).

[f] Maximum *J* value included in the database for the *P*, *Q* and *R* branches of each band.

[g] HITRAN, EDB17 – the band was completed using indicated source [1,2]. “Exp. P” – perturbed band, measured line positions were used for intensity calculations and in the recommended line list.

Fig. 1

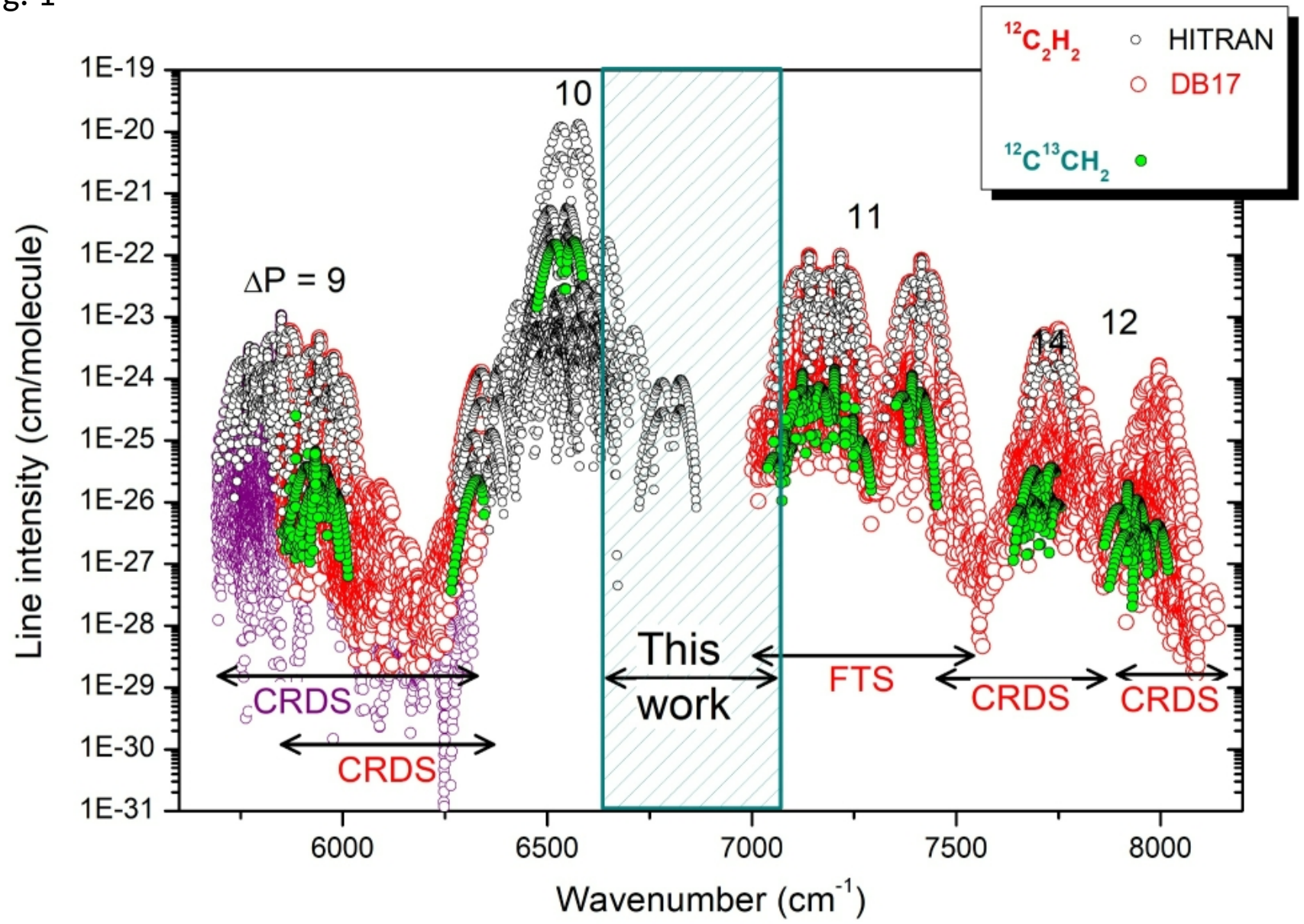
$^{12}C_2H_2$
HITRAN
DB17
$^{12}C^{13}CH_2$
10
11
12
14
ΔP = 9
This work
CRDS
CRDS
FTS
CRDS
CRDS
Line intensity (cm/molecule)
Wavenumber (cm^{-1})
1E-19
1E-20
1E-21
1E-22
1E-23
1E-24
1E-25
1E-26
1E-27
1E-28
1E-29
1E-30
1E-31
6000
6500
7000
7500
8000

Fig. 2

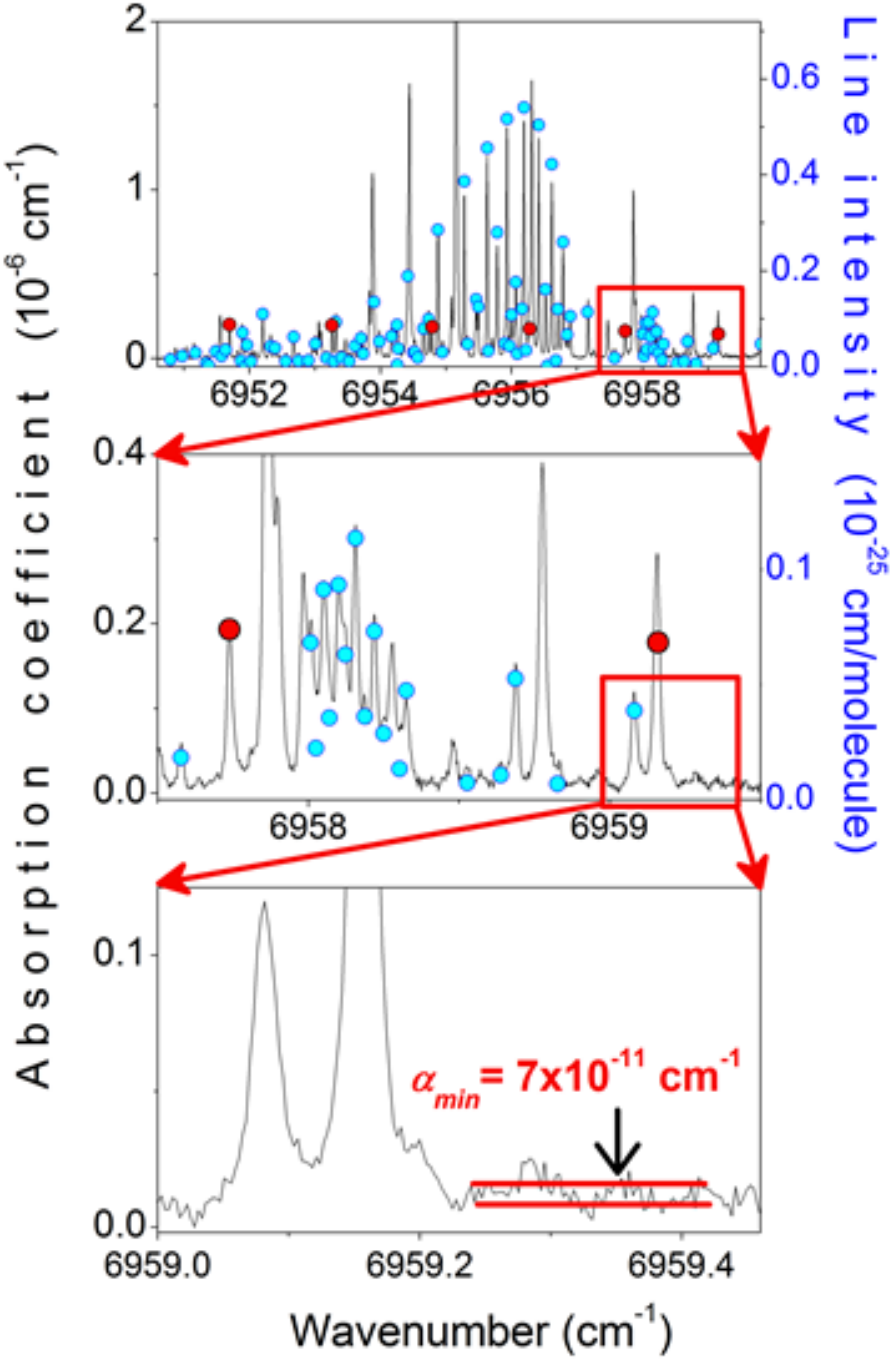
Absorption coefficient (10^{-6} cm^{-1})
Line intensity (10^{-25} cm/molecule)
Wavenumber (cm^{-1})
α_{min} = 7x10^{-11} cm^{-1}
6952
6954
6956
6958
6959
6959.0
6959.2
6959.4

Fig. 3

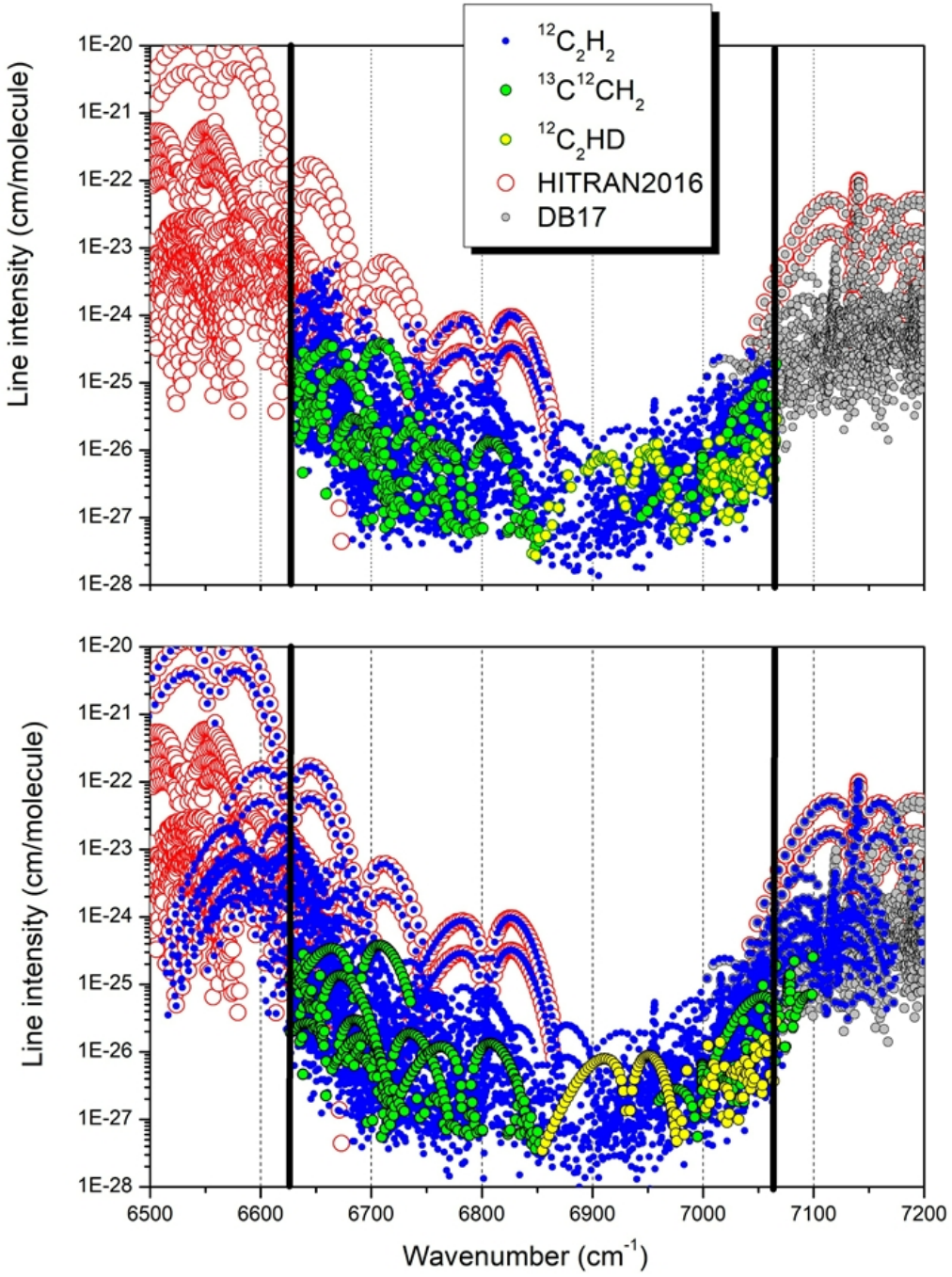
$^{12}C_2H_2$
$^{13}C^{12}CH_2$
$^{12}C_2HD$
HITRAN2016
DB17
Line intensity (cm/molecule)
1E-20
1E-21
1E-22
1E-23
1E-24
1E-25
1E-26
1E-27
1E-28
6500
6600
6700
6800
6900
7000
7100
7200
Wavenumber (cm^{-1})

Fig. 4

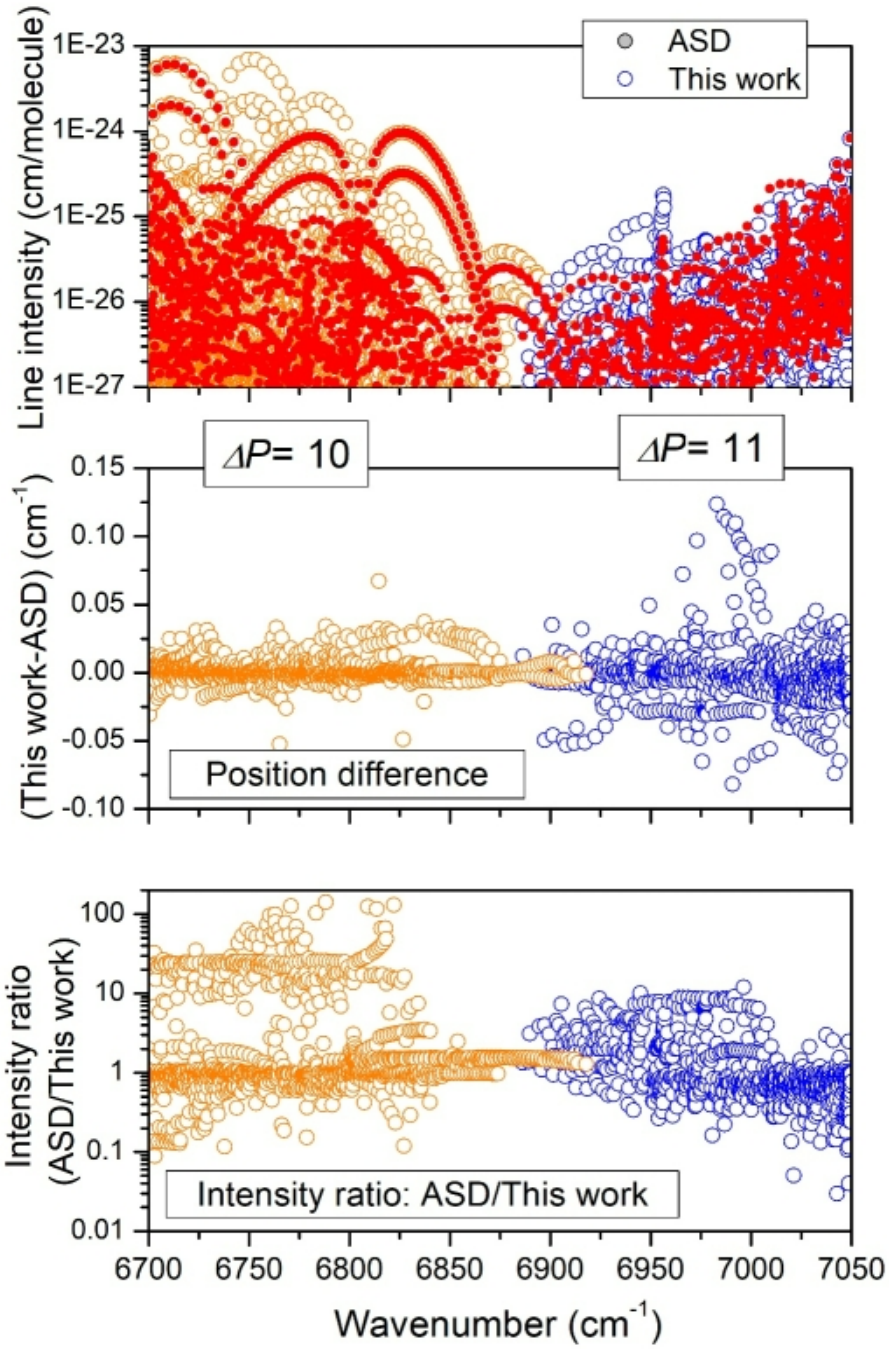
ASD
This work
Line intensity (cm/molecule)
1E-23
1E-24
1E-25
1E-26
1E-27
ΔP= 10
ΔP= 11
(This work-ASD) (cm-1)
0.15
0.10
0.05
0.00
-0.05
-0.10
Position difference
Intensity ratio (ASD/This work)
100
10
1
0.1
0.01
Intensity ratio: ASD/This work
6700
6750
6800
6850
6900
6950
7000
7050
Wavenumber (cm-1)

Fig. 5

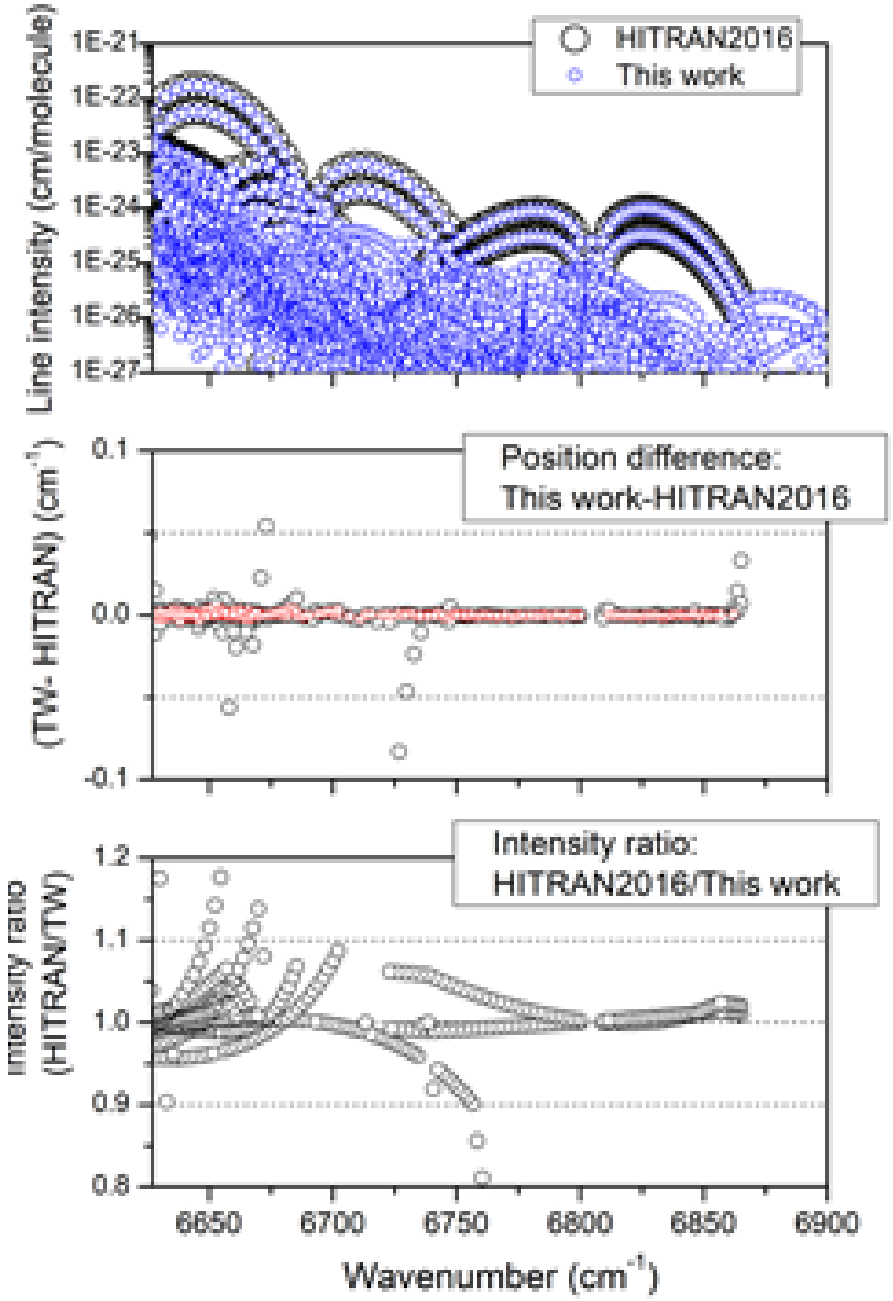
HITRAN2016
This work
Line intensity (cm/molecule)
1E-21
1E-22
1E-23
1E-24
1E-25
1E-26
1E-27
Position difference:
This work-HITRAN2016
(TW- HITRAN) (cm-1)
0.1
0.0
-0.1
Intensity ratio:
HITRAN2016/This work
Intensity ratio
(HITRAN/TW)
1.2
1.1
1.0
0.9
0.8
6650
6700
6750
6800
6850
6900
Wavenumber (cm-1)

The authors declare that they have no known competing financial interests or personal relationships that could have appeared to influence the work reported in this paper.